

Dihydroquinazolines as a Novel Class of *Trypanosoma brucei* Trypanothione Reductase Inhibitors: Discovery, Synthesis, and Characterization of their Binding Mode by Protein Crystallography

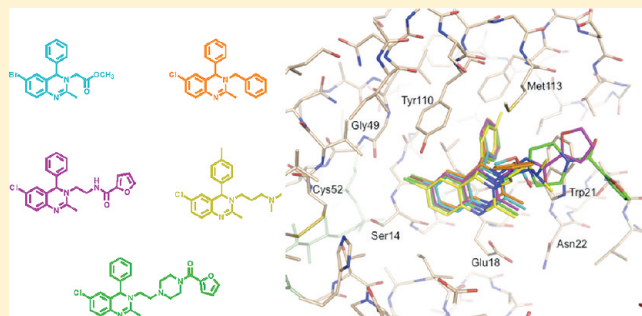
Stephen Patterson,^{†,§} Magnus S. Alpey,^{†,§} Deuan C. Jones,[†] Emma J. Shanks,[†] Ian P. Street,[‡] Julie A. Frearson,[†] Paul G. Wyatt,[†] Ian H. Gilbert,[†] and Alan H. Fairlamb^{*,†}

[†]Division of Biological Chemistry and Drug Discovery, College of Life Sciences, University of Dundee, Dow Street, Dundee DD1 5EH, U.K.

[‡]The Walter and Eliza Hall Institute of Medical Research, 1G Royal Pde, Centre for Drug Candidate Optimisation, Monash Institute of Pharmaceutical Sciences, Monash University (Parkville Campus), Parkville VIC-3052, Australia

S Supporting Information

ABSTRACT: Trypanothione reductase (TryR) is a genetically validated drug target in the parasite *Trypanosoma brucei*, the causative agent of human African trypanosomiasis. Here we report the discovery, synthesis, and development of a novel series of TryR inhibitors based on a 3,4-dihydroquinazoline scaffold. In addition, a high resolution crystal structure of TryR, alone and in complex with substrates and inhibitors from this series, is presented. This represents the first report of a high resolution complex between a noncovalent ligand and this enzyme. Structural studies revealed that upon ligand binding the enzyme undergoes a conformational change to create a new subpocket which is occupied by an aryl group on the ligand. Therefore, the inhibitor, in effect, creates its own small binding pocket within the otherwise large, solvent exposed active site. The TryR–ligand structure was subsequently used to guide the synthesis of inhibitors, including analogues that challenged the induced subpocket. This resulted in the development of inhibitors with improved potency against both TryR and *T. brucei* parasites in a whole cell assay.



INTRODUCTION

The neglected disease human African trypanosomiasis (HAT), or African sleeping sickness, is caused by two subspecies of the protozoan parasite *Trypanosoma brucei*. If not successfully treated, HAT is fatal, and it is estimated to be responsible for about 30000 deaths each year in sub-Saharan Africa.¹ There is no effective vaccine for HAT, and the current therapeutics used to treat the disease possess a number of limitations including high toxicity, efficacy against only a single *T. brucei* subspecies, and the emergence of resistance.^{1,2} Undoubtedly, there is an urgent need for the identification and development of new antitrypanosomal compounds.

T. brucei and a number of related parasites utilize a redox metabolism based around the dithiol trypanothione [*N*¹,*N*⁸-bis(glutathionyl)spermidine] (Figure 1), which is absent in humans.³ Therefore, the enzymes involved in this redox pathway are considered to be attractive targets for the development of new antitrypanosomal drugs.^{4,5} One component of the trypanothione-based redox pathway is trypanothione reductase (TryR, EC 1.8.1.12), an NADPH-dependent disulfide oxidoreductase, which is responsible for reducing trypanothione disulfide (T[S]₂) to dihydro-trypanothione (T[SH]₂) (Figure 1).³

This reduction is analogous to that performed by glutathione reductase (GR, EC 1.8.1.7) in most organisms, including humans. However, the active sites of the two enzymes have opposite net charges, facilitating the development of inhibitors selective for TryR over GR.⁶ Trypanothione provides reducing equivalents either directly or via tryparedoxin for several essential enzymes that protect *T. brucei* parasites from oxidative damage.⁷

Genetic studies have demonstrated that TryR activity is essential for *T. brucei* parasites to grow in culture and to be infective in an animal disease model.⁸ Therefore, TryR is a genetically validated drug target, one important criterion in drug target assessment.^{9,10} In addition, TryR inhibitors with diverse core-scaffolds have been reported.^{9,11–19} However, many of the reported inhibitors are of low potency (TryR IC₅₀ >1 μM), or are not drug-like (e.g., mol wt >500) and therefore do not represent suitable starting points for the development of antitrypanosomal drugs. This requirement for high molecular weight compounds to effectively inhibit TryR may in part be a consequence of

Received: March 18, 2011

Published: August 18, 2011

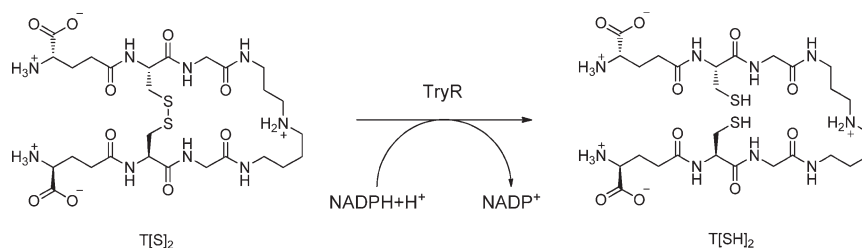


Figure 1. The TryR-catalyzed reduction of trypanothione disulfide (T[S]₂) to dihydrotrypanothione (T[SH]₂, N¹,N⁸-bis(glutathionyl)spermidine).

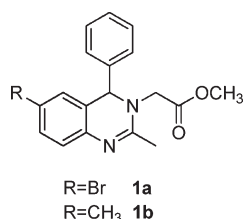


Figure 2. 3,4-Dihydroquinazolines **1a** and **1b**, small molecule inhibitors of *T. cruzi* and *T. brucei* TryR (see Table 1).

the large, solvent-exposed trypanothione-binding site of the enzyme.²⁰

Although it has been possible to readily identify TryR inhibitor series by both high-throughput^{9,13} and virtual screening,^{21,22} the development of these hits into submicromolar inhibitors has been limited by the lack of crystallographic information required to guide structure-based drug design. None of the proposed TryR–inhibitor binding modes derived from docking experiments^{11,21,23–25} have been verified by structural techniques and the only high-resolution TryR–inhibitor complex that has been reported is that from a covalent adduct between quinacrine mustard and *T. cruzi* TryR.²⁶

In this current article, we report the synthesis and evaluation of a series of novel *T. brucei* TryR inhibitors based on the 3,4-dihydroquinazolinone core structure (Figure 2). This series was identified from a high-throughput screen against *Trypanosoma cruzi* TryR¹³ and subsequently confirmed to also inhibit *T. brucei* TryR. Inhibition data are reported for all analogues against *T. brucei* TryR and for selected compounds against the parasite in a whole cell assay. The structure–activity relationship (SAR) derived from the *in vitro* data is discussed. Additionally, the key molecular interactions formed between the 3,4-dihydroquinazolines and TryR have been identified by determining the X-ray crystal structure of inhibitors in complex with *T. brucei* TryR. The liganded structures were used to guide further synthesis, resulting in the preparation of analogues with increased potency against the target enzyme.

CHEMISTRY

The general synthetic route used to access the 3,4-dihydroquinazolinone analogues is outlined in Scheme 1. This route was based on a modification of a literature route for the preparation of 2-trifluoromethyl-3,4-dihydroquinazolines.²⁷ Briefly, substituted 2-aminobenzophenones (**2a–d**) were converted to amides (**3a–d**) by treatment with functionalized acid chlorides. The ketone functionality of **3a–d** was subsequently reacted with primary amines under microwave irradiation to afford substituted imines (**4a–k**, **7a–d**, **10**, **12**, **14b–d**, **20**). Reduction of the

imines with NaBH₄ gave the corresponding secondary amines, from which the 3,4-dihydroquinazolines could be accessed either by reaction with POCl₃ or by temperature-assisted cyclization. Alternatively, both the imine reduction and cyclization reactions could be achieved in a single pot by treating the imines with NaBH₄ in refluxing EtOH (Scheme 1). This synthetic route proved to be tolerant of a variety of substituents and was used to prepare a number of small compound arrays and individual compounds. The full range of compounds prepared is shown in Tables 2–5.

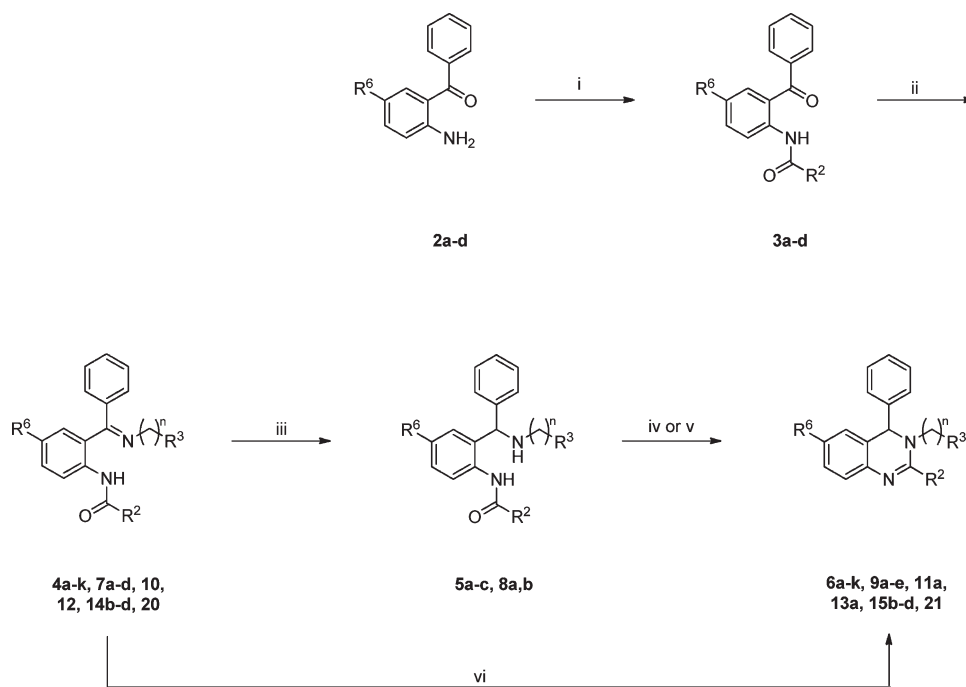
To prepare two small collections of substituted amide analogues (Scheme 2) the *t*-Boc-protected analogues **11a** and **13a** were first prepared by following the chemical transformations outlined above (Scheme 1). Deprotection of **11a** and **13a** by treatment with excess HCl, followed by reaction of the resultant amines with a collection of acid chloride building blocks, gave amides **11b–h** and **13b–h**, respectively (Scheme 2).

Variation at the R⁶ position required the synthesis of intermediate 5-substituted-benzophenones. Where R⁶ was halogen (**15c** and **15d**), this was obtained by regioselective halogenation of 2-aminobenzophenone²⁸ (Scheme S4 of the Supporting Information). Using the 6-bromo derivative (**15c**), it was possible to introduce aromatic rings at the 6-position using Suzuki chemistry²⁹ (Scheme 3). Similarly, reaction of the 8-bromo-derivative **18** under Suzuki reaction conditions²⁹ gave the 8-phenyl analogue (**19**) (Scheme 3).

To further investigate the series, it was necessary to prepare analogues where the substituent R⁴ was varied. This required substituted 2-aminobenzophenone starting materials, which were synthesized by three different routes (Scheme 4). Following a literature sequence, anthranilate **23** was converted to benzoxazinone **24**³⁰ and subsequently reacted with *p*-tolylmagnesium bromide to give benzophenone **27a** in an 18% yield.³¹ Benzophenone **27a** was then converted to quinazolinone analogue **29a** using the general reaction sequence described above. Given the poor yield of **27a**, an improved two-step synthesis was employed for the preparation of **27b–e** (Scheme 4). Briefly, anthranilate **23** was treated with substituted aryl lithiums followed by TMSCl to give the substituted 2-aminobenzophenones **26b–e**.³² Subsequent reaction with AcCl gave amides **27b–e**, which were converted to **29b–e** as outlined in Scheme 4. Alternatively, benzophenone analogues could be accessed by reacting Grignard reagents with nitrile **25**, followed by hydrolysis of the resultant imine (Scheme 4). This was useful for the preparation of analogues that were not accessible by other routes (Scheme S6 of the Supporting Information).

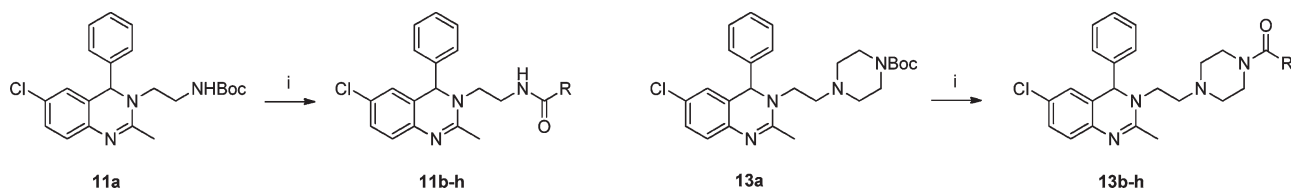
The route used to prepare each of **29b–f** required four dedicated steps from **23**, or **25** making this route unsuitable for the rapid generation of analogues. Therefore, a shorter, more suitable route (Scheme 5) was developed for the preparation of a

Scheme 1. General Synthetic Route to 3,4-Dihydroquinazoline Analogues (Also See Schemes S1, S3, and S4 of the Supporting Information; For Details of Individual Substituents, See Tables 2–5; Note That Products of This Route Are Racemates)^a



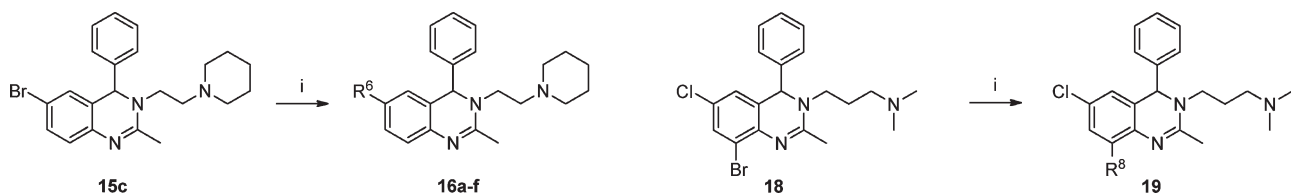
^a Reagents and conditions: (i) R^2COCl , DMAP, pyridine, CH_2Cl_2 , 25 °C, 16 h; (ii) $H_2N(CH_2)_nR^3$, EtOH, 160 °C (MW), 2 h; (iii) $NaBH_4$, DMF, or EtOH, 50 °C, 16 h; (iv) $POCl_3$, CH_2Cl_2 , 0–25 °C, 16 h; (v) EtOH, 160 °C (MW) 2 h; (vi) $NaBH_4$, EtOH, 78 °C, 16 h.

Scheme 2. Synthetic Routes for the Preparation of Two 3,4-Dihydroquinazoline Amide Arrays (For Additional Details, See Scheme S3 of the Supporting Information; For Details of Individual Substituents, See Table 3)^a



^a Reagents and conditions: (i) (1) HCl, dioxane/THF, 25 °C, 2 h; (2) $RCOCl$, pyridine, CH_2Cl_2 , 40 °C, 16 h.

Scheme 3. Synthetic Routes for the Preparation of Bi-aryl 3,4-Dihydroquinazoline Analogues (See Schemes S4 and S5 of the Supporting Information for the Synthesis of 15c and 18, Respectively; For Details of Individual Substituents, See Table 4)^a

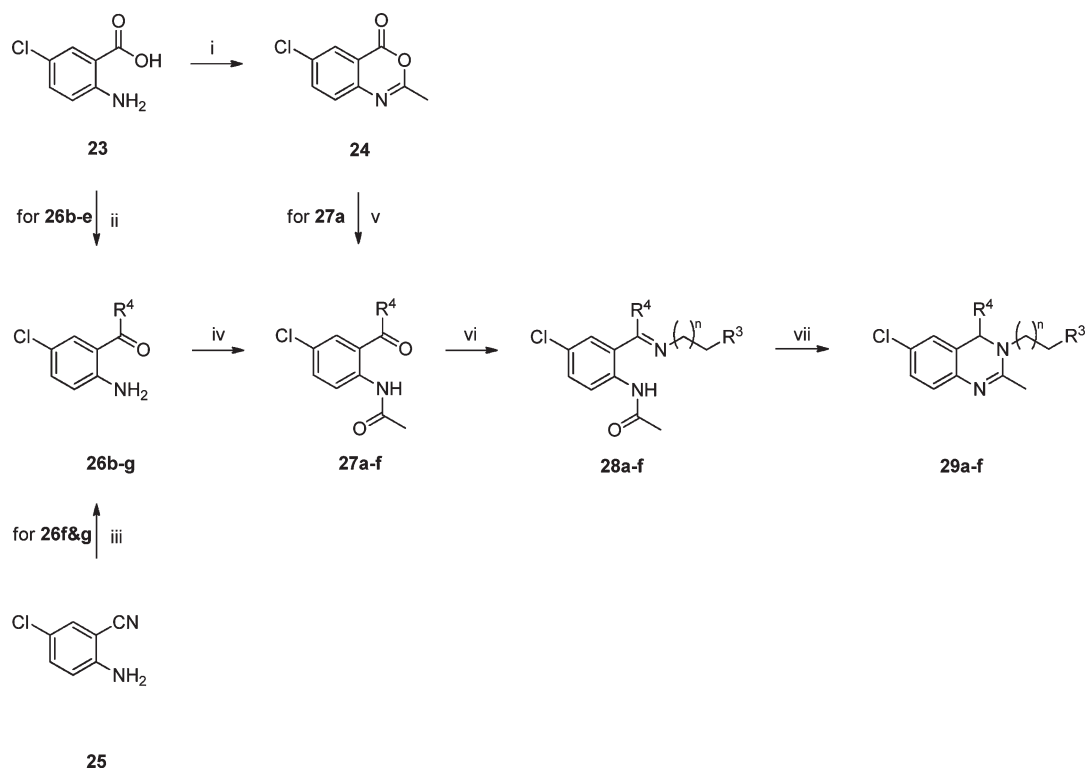


^a Reagents and conditions: (i) $(HO)_2B-R^{6/8}$, K_3PO_4 , $Pd(PPh_3)_4$, dioxane/ H_2O , 120 °C (MW), 0.5 h.

small collection of R^4 analogues (32a–g). Benzoxazinone 24 was converted into quinazolinone 30 by reaction with 1-(2-aminoethyl)piperidine and subsequent microwave-assisted cyclocondensation.³³ Reaction of 30 with either substituted phenyl Grignard reagents or benzylmagnesium chloride afforded the 4-substituted 3,4-dihydroquinazolin-4-ols 31a–h.³⁴ However, the attempted

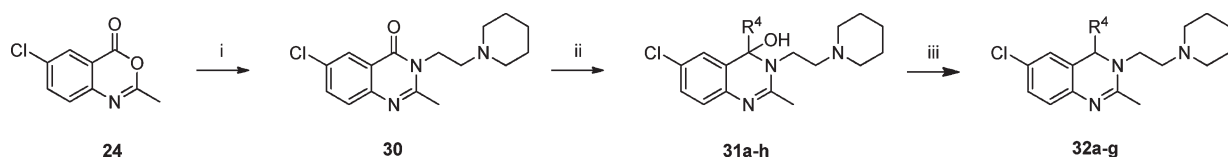
reactions between 30 and cyclohexylmagnesium or cyclopentylmagnesium chloride were unsuccessful, suggesting a limitation in the range of R^4 groups that could be incorporated via this route. Benzylic alcohols 31a–g were subsequently reduced by treatment with Et_3SiH and $BF_3 \cdot OEt_2$ to give the desired 3,4-dihydroquinazolines 32a–g.

Scheme 4. Synthetic Routes for the Preparation of 3,4-Dihydroquinazoline Analogues Containing Different Substitutions at R⁴ (29a–f) (Also See Scheme S7 of the Supporting Information; For Details of Individual Substituents, See Table S)^a



^a Reagents and conditions: (i) Ac₂O, 138 °C, 2 h; (ii) (1) R⁴Li, THF, 0 °C, 2 h; (2) TMSCl, 0–25 °C, 15 min; (iii) R⁴ MgX, Et₂O, 0–25 °C, 16 h; (iv) AcCl, DMAP, pyridine, CH₂Cl₂, 25 °C, 16 h; (v) R⁴ MgX, THF, 25 °C, 30 min, 67 °C, 2 h; (vi) H₂N(CH₂)_nCH₂R³, EtOH, 160 °C (MW), 2 h; (vii) NaBH₄, EtOH, 78 °C, 16 h.

Scheme 5. Shortened Synthetic Strategy for the Preparation of 3,4-Dihydroquinazoline Analogues Substituted at R⁴ (For Details of Individual Substituents, See Table S)^a



^a Reagents and conditions: (i) (1) 1-(2-aminoethyl)piperidine, CH₂Cl₂, 25 °C, 1 h; (2) formamide, 130 °C (MW), 10 min; (ii) R⁴ MgCl, THF, 0–25 °C, 2–4 h; (iii) BF₃·OEt, HSiEt₃, CH₂Cl₂, 25 °C, 16 h.

The two C4 methoxyphenyl analogues (32c and 29d) were converted into the corresponding phenol analogues (35 and 36) by treatment with BBr₃ (Scheme S8 of the Supporting Information). This gave a total of 15 analogues containing different C4 substitutions (Table S).

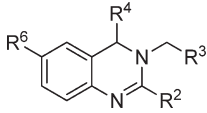
■ BIOLOGICAL ASSAYS

Compounds were assayed against recombinant *T. brucei* TryR using a spectrophotometric nonenzymatically coupled assay.^{35,36} In this assay, the activity of TryR is coupled to the reduction of DTNB (5,5'-dithiobis-(2-nitrobenzoic acid)) to 2TNB⁻, which can be measured as an increase in absorbance at 412 nm (Figure S1 of the Supporting Information). The same assay was used to conduct a more detailed kinetic analysis in order to determine the mode of inhibition of selected inhibitors (see section 2.2 of the

Supporting Information for more details). Selected compounds were also assayed against bloodstream form *T. brucei* using the resazurin fluorescence-based cell viability assay³⁷ modified from a previous method.³⁸ In addition, the compounds were assayed using a similar protocol against MRC-5 cells as an indicator of mammalian toxicity. Compound 1a was also assayed against human GR using a protocol conceptually similar to the TryR assay.

■ RESULTS AND DISCUSSION

Identification and Validation of the 3,4-Dihydroquinazolines as a Hit Series. A high-throughput screen of 100000 compounds against *T. cruzi* TryR¹³ identified the 3,4-dihydroquinazolines 1a and 1b (Figure 2, Table 1) as low potency inhibitors

Table 1. Inhibitory Activities of Commercially Available 3,4-Dihydroquinazoline Analogues against *T. brucei* TryR


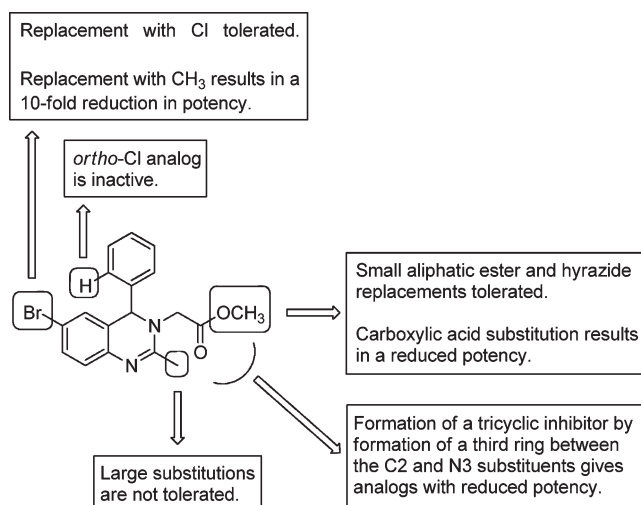
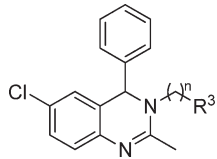
	R ²	R ³	R ⁴	R ⁶	TryR IC ₅₀ (μM)
1a	CH ₃	CO ₂ CH ₃	Ph	Br	6.8 ^a
1b	CH ₃	CO ₂ CH ₃	Ph	CH ₃	67 ^b
1c	CH ₃	CO ₂ CH ₃	Ph	Cl	9.4
1d	CH ₃	CO ₂ CH ₃		Br	>100
1e	CH ₃	CO ₂ CH ₂ CH ₃	Ph	Br	12
1f	CH ₃	CO ₂ H	Ph	Br	37
1g	CH ₃	CONHNH ₂	Ph	Br	15
1h	CH ₂ CH ₃	CO ₂ CH ₃	Ph	Br	23
1i	CH ₂ -N-morpholine	CO ₂ CH ₃	Ph	Br	89
1j	CH ₂ CH ₂ -N-morpholine	CO ₂ CH ₃	Ph	Br	93
1k	Ph	CO ₂ CH ₃	Ph	CH ₃	>100
1l	3,4,5-OCH ₃ phenyl	CO ₂ CH ₃	Ph	CH ₃	>100
1m	-CH ₂ NHCO-		Ph	Br	37
1n	-CH ₂ CH ₂ NHCO-		Ph	Br	39

^a *T. cruzi* TryR IC₅₀ = 19 μM. ^b *T. cruzi* TryR IC₅₀ = 38 μM.

(IC₅₀ 19 and 38 μM, respectively). The 3,4-dihydroquinazolines were considered promising screening hits for further investigation due to their low molecular weights (373 and 308), reasonable ligand efficiencies (0.28 and 0.27 kcal mol⁻¹ per non-H atom, respectively), and low polar surface area, an important property due to the requirement for blood-brain barrier permeability to treat stage 2 HAT. (As defined here, ligand efficiency = free energy of binding (ΔG)/number of non-hydrogen (“heavy”) atoms, where ΔG = -RT · lnK_d with R = 1.987 cal K⁻¹ mol⁻¹; T = 300 K; and assuming K_d ~ IC₅₀ (M).)

To determine the validity of this series as a starting point for the development of a lead compound for the treatment of HAT, **1a**, **1b**, and a small collection of commercially available analogues (**1c–n**) were assayed against *T. brucei* TryR (Table 1). The hit compounds **1a** and **1b** were found to have IC₅₀ values of 6.8 and 67 μM, respectively, confirming their activity against the *T. brucei* enzyme. The similar levels of activity observed for **1a** and **1b** against *T. cruzi* and *T. brucei* TryR (<3-fold difference) is as expected given the high degree of sequence identity between TryR in the two species (83% at the amino acid level overall, 100% for active site residues). The remainder of the commercial analogues (**1c–n**) display a range of TryR inhibitory activities (IC₅₀ 9.4 to >100 μM, Table 1). Although no analogues with improved potency were identified, it was possible to develop a preliminary SAR analysis (Figure 3). Therefore, the 3,4-dihydroquinazolines represent a validated TryR inhibitor series and a hit expansion program was initiated.

Biological Characterization of the Hit Series. A more detailed kinetic analysis (Figure S2 of the Supporting Information) established that **1a** is a linear competitive inhibitor of TryR (with respect to trypanothione disulfide), with a K_i value of 0.92 ± 0.06 μM, in reasonable agreement with the IC₅₀ value determined in the high-throughput assay (Table 1). Therefore, it is possible that the 3,4-dihydroquinazolines are binding to TryR in an orientation that partially occludes the substrate binding

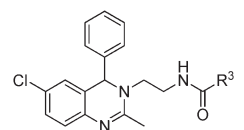
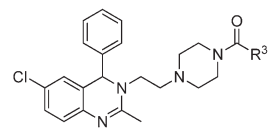
**Figure 3. SAR derived from screening analogues 1a–n (Table 1).****Table 2. N3-Substituted 3,4-Dihydroquinazoline Analogues and Their Inhibitory Activities against *T. brucei* TryR and in Cell-Based Assays**


	R ³	n	IC ₅₀ (μM)		EC ₅₀ (μM)	
			TryR	<i>T. brucei</i>	MRC5	
1c	CO ₂ Me	1	9.4			
6a	Ph	1	0.93	13	46	
6b	Ph	2	2.0			
6c	2-OMe-Ph	1	1.1			
6d	2-F-Ph	1	0.94	14	36	
6e	3-Cl-Ph	1	3.5			
6f	3-CF ₃ -Ph	1	1.5			
6g	3-NMe ₂ -Ph	1	0.81	6.4	27	
6h	4-Me-Ph	1	1.3			
6i	4-Cl-Ph	1	2.2			
6j	4-CF ₃ -Ph	1	2.2			
6k	Me	1	1.2			
9a	N-piperidine	2	1.8	1.3	14	
9b	N-morpholine	2	2.8			
9c	N-4-Me-piperazine	2	0.93 ^a	4.4	4.6	
9d	NMe ₂	2	3.5			
9e	NMe ₂	3	1.0	2.7	2.7	
9f	NHMe	2	2.0			
21	OH	2	1.7			

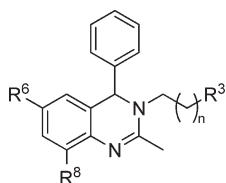
^a TryR K_i = 0.32 ± 0.01 μM.

pocket. Compound **1a** is a selective TryR inhibitor because it was inactive against human GR (IC₅₀ >100 μM), the nearest human homologue of TryR. This is consistent with **1a** binding to the negatively charged substrate-binding pocket of TryR, in contrast

Table 3. Substituted Amide 3,4-Dihydroquinazoline Analogues and Their Inhibitory Activities against *T. brucei* TryR and in Cell-Based Assays

Scaffold	Cmpd	R ³	IC ₅₀	EC ₅₀ (μM)	
			(μM) TryR	<i>T. brucei</i>	MRC5
	11a	O ^t Bu	2.6	-	-
	11b	Me	2.1	-	-
	11c	^c Pr	2.3	-	-
	11d	Ph	1.7	-	-
	11e	2-furan	0.86 ^a	19	22
	11f	CH ₂ Ph	1.8	-	-
	11g	CH ₂ OMe	1.3	-	-
	11h	CH ₂ NMe ₂	0.81	13	12
		13a	O ^t Bu	1.5	-
13b		Me	1.7	-	-
13c		^c Pr	1.5	-	-
13d		Ph	1.6	-	-
13e		2-furan	0.42	10	23
13f		CH ₂ Ph	2.0	-	-
13g		CH ₂ OMe	1.6	-	-
13h		CH ₂ NMe ₂	0.37 ^b	5.6	6.0

^a TryR $K_i = 0.44 \pm 0.03 \mu\text{M}$, $K_i' = 2.27 \pm 0.3 \mu\text{M}$. ^b TryR $K_i = 0.27 \pm 0.02 \mu\text{M}$, TryR $K_i' = 1.78 \pm 0.3 \mu\text{M}$.

Table 4. C6-Substituted and C8-Substituted 3,4-Dihydroquinazoline Analogues and Their Inhibitory Activities against *T. brucei* TryR and in Cell-Based Assays

n	R ³	R ⁶	R ⁸	IC ₅₀ (μM)	EC ₅₀ (μM)	
				TryR	<i>T. brucei</i>	MRC5
9a	1 N-piperidine	Cl	H	1.8	1.3	14
15b	1 N-piperidine	H	H	0.78	12	23
15c	1 N-piperidine	Br	H	0.79	0.44	8.4
15d	1 N-piperidine	I	H	0.35	0.55	6.8
16a	1 N-piperidine	Ph	H	7.3	0.75	3.4
16b	1 N-piperidine	4-pyridine	H	4.4		
16c	1 N-piperidine	2-furan	H	1.3		
16d	1 N-piperidine	3-thiophene	H	0.79		
16e	1 N-piperidine	1-naphthyl	H	8		
16f	1 N-piperidine	2-benzo(b)furan	H	8.5		
18	2 NMe ₂	Cl	Br	53		
19	2 NMe ₂	Cl	Ph	24		

to the positively charged pocket in GR. Analogue **1a** was assayed against bloodstream form *T. brucei* and found to have an EC₅₀ of 40 μM representing a >5-fold reduction in potency between the biochemical and cell assay. In a counter-screen against a mammalian cell line (MRC5 cells), **1a** was found to be inactive (EC₅₀ >50 μM). This is consistent with **1a** being inactive against GR.

Hit Expansion. Screening of commercial analogues demonstrated that the C6-bromine could be replaced with a chlorine atom without a significant loss of activity (**1a** vs **1c**, Table 1). This beneficial reduction in molecular weight together with the availability of starting material **2a** resulted in all further compound arrays consisting of analogues with a C6-chlorine substitution (except where C6 was the point of variation). Initial synthesis aimed to identify a replacement for the potentially labile ester functionality of **1c**. Therefore, benzyl analogues **6a–j**, amine analogues **9a–f**, and alcohol-containing analogue **21** were prepared (Table 2, Scheme 1, and Schemes S1 and S2 of the Supporting Information). Analogues **6a–j**, **9a–f**, and **21** all demonstrated an improved potency with respect to ester **1c** in the *T. brucei* TryR assay, including examples showing a 10-fold improvement (**6a**, **6d**, **6g**, and **9c**). However, there is only a 4-fold difference in potency between the most and least potent analogues in the two arrays (**6g** vs **6e/9d**), resulting in a flat SAR.

To improve potency, a chemistry-driven, systematic SAR analysis was performed to investigate the N3-, C4-, C6-, and C8-positions. Additional functionality at the C2-position had been shown to result in a large reduction of potency (**1i–1l**, Table 1, Figure 3), so was not further investigated.

To probe the N3-position, amide derivatives of analogues **9f** and **9c** were prepared (**11a–h** and **13a–h**, Scheme 2 and Scheme S3 of the Supporting Information). These amides retained their TryR inhibitory activity (Table 3), but there was a narrow range of potencies (IC₅₀ 0.37–2.6 μM), giving no identifiable SAR. Compounds **11e** and **13h** were found to have a mixed mode of inhibition, although comparison of their K_i and K_i' values show that they bind to the free enzyme more readily than to the enzyme–T[S]₂ complex, similar to the mode of inhibition of **1a**. Although more potent, the ligand efficiencies³⁹ of **13e** and **13h** are poorer than that of **9c** (0.27 and 0.28 vs 0.31 kcal mol⁻¹ per non-H atom, respectively).

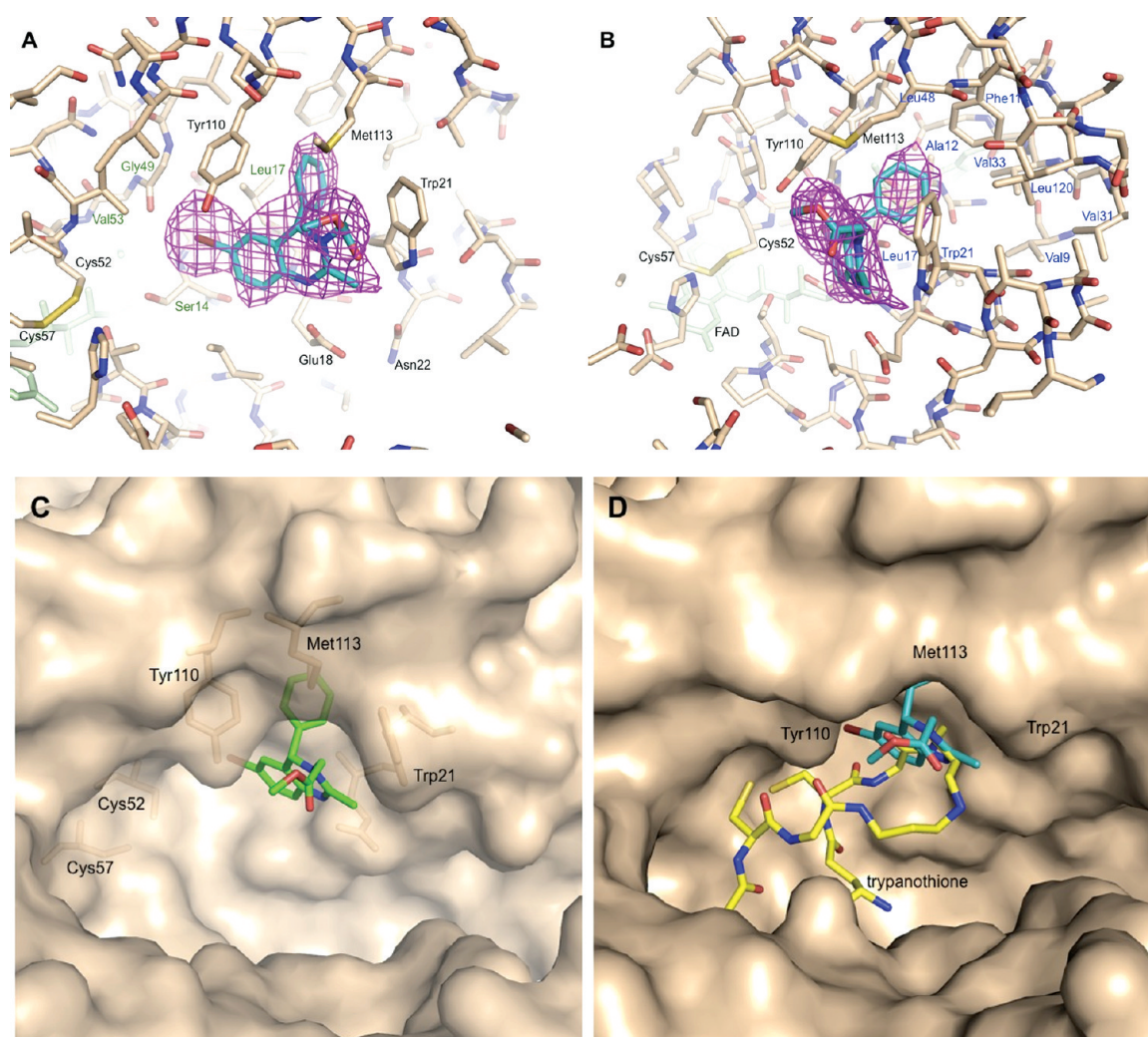


Figure 4. The X-ray protein crystal structure of **1a** in complex with *T. brucei* TryR. (A) and (B) show two orientations, rotated about 90° , of the TryR–compound **1a** complex active site showing experimental density (magenta) for the inhibitor contoured at 2.5σ . Compound **1a** is shown in blue and FAD in turquoise. Carbon atoms are shown in brown, oxygens in red, nitrogens in dark blue, and sulfurs in yellow. Important residues have been highlighted in black including Trp21 and Met113, forming the hydrophobic wall and electron donor Glu18. Those residues involved in binding the halogen component are labeled in green, and those involved in the novel hydrophobic pocket are in blue. (C) Shows the same complex with the solvent accessible surface shown in beige and the ligand in green to demonstrate where the inhibitor is occupying subpockets within the active site cleft. (D) Surface representation of TryR active site cleft with bound compound **1a**. The structure of T[SH]₂ (yellow) bound to TryR from PDB entry 2w0w has been overlaid.

When investigating the C6-position (Scheme 3, Table 4), the N3 ester was replaced with a more potent basic moiety (e.g., **9a** vs **1c**). The potency of analogues **1a** and **15c** demonstrated that a bromine atom was tolerated at C6 (Tables 1 and 4). Therefore, the C6-position was explored by introducing aryl substituents, prepared as outlined in Scheme 3. The C6-aryl analogues all demonstrated low micromolar TryR IC₅₀ values (Table 4), giving no significant improvement in potency. It was observed that the furan and thiophene analogues (**16c** and **16d**) were 5- to 10-fold more potent than the other C6-aryls (**16a,b,e,f**). The fact that analogues containing large bicyclic substitutions at C6 retain some activity (**16e,f**) suggests that the protein does not entirely occlude the C6 position of the inhibitor upon binding. In addition, the observation that the C6-bromine analogue (**15c**) is 10-fold more potent than the similarly sized C6-phenyl analogue (**16a**) implies that the beneficial effect of a

bromine substitution is not entirely due to its steric bulk and hydrophobic character.

The C8-substituted analogues (**18** and **19**) were significantly less active when assayed against TryR (Table 4), suggesting that the introduction of a large hydrophobic group at C8 is detrimental to the inhibitor's ability to bind to TryR.

As the chemistry-driven approach failed to identify inhibitors with improved ligand efficiency, protein crystallographic investigations were initiated in order to facilitate an alternative rational inhibitor design program. The SAR expanded to include the analogues in Tables 2–4 above is summarized in Figure S3 of the Supporting Information.

X-ray Crystallography, Analysis of Ligand Binding, and Rationalization of SAR. The X-ray crystal structure for the hit compound **1a** in complex with *T. brucei* TryR was solved and refined at a resolution of 2.8 \AA with an R factor and R_{free} of 16.4% and 21.9%, respectively (Figure 4A,B, Table S1 of the Supporting Information).

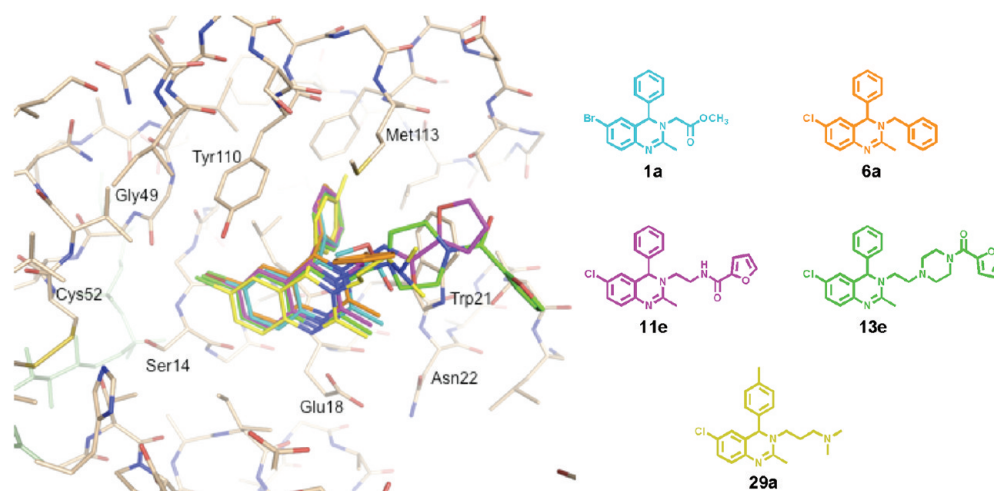


Figure 5. The crystallographically determined binding orientations of compounds **6a**, **11e**, **13e**, and **29a** overlaid in the active site of the TryR–**1a** complex structure. **1a** is displayed in cyan, **6a** in orange, **11e** in magenta, **13e** in green, and **29a** in yellow. The 3,4-dihydroquinazoline and phenyl ring systems overlay well, while the more variable and flexible N3-substituents point out into the active site opening in a variety of orientations.

This represents the first report of a high resolution noncovalent small molecule–protein X-ray crystal structure for TryR. In addition, the X-ray crystal structures of nonliganded TryR (2woi), TryR in complex with NADPH (2wov), and TryR in complex with trypanothione dithiol and NADPH (2wow) have been determined. All of the TryR structures reported herein are in complex with FAD. Ramachandran analyses of the structures show more than 99% of residues are in the allowed regions in all models. The few residues outside these regions correspond to Tyr45, which is known to reside in a strained loop region of all other TryR structures and Arg331, the main chain of which is also held in a strained conformation in some TryR structures. See the Supporting Information (sections 3.2–3.5) for a detailed discussion of the comparison between the *T. brucei* TryR X-ray structures reported in this manuscript and other TryR structures previously reported in the literature.

Examination of the TryR–**1a** complex revealed that the ligand binds in a region of the enzyme's active site cleft that would normally be occupied by the Gly-I and spermidine moieties of T[S]₂ (Figure 4D). Therefore, the observed binding mode is consistent with the mode of inhibition of **1a** being competitive with respect to T[S]₂ as described above.

The most interesting feature of the TryR–**1a** structure is the observation that the enzyme undergoes an induced conformational change upon inhibitor binding. This conformational change generates a new subpocket within the active site, which accommodates the C4-phenyl of **1a** (Figure 4C). Previously, the active site of TryR was believed to be a rigid structure,⁴⁰ formed by residues that belong to a congregation of α -helices. Accordingly, the substrate T[S]₂ is highly flexible and adopts a conformation to accommodate the rigid active site. However, upon binding of **1a**, the Met113 side chain moves approximately 5 Å outward into the active site, creating a new hydrophobic pocket. This subpocket is lined by Leu120, Phe114, Val33, Leu17, Ala12, Val9, Val31, and Leu48. The entrance to the subpocket is “guarded” by Trp21, Met113, and Tyr110. This induced fit had not previously been predicted in TryR, and the significant movement of the Met113 side chain clearly changes the properties of the active site, thus affecting the binding of T[S]₂. The bound inhibitor not only sterically impedes the binding of the

spermidine moiety of T[S]₂ but also alters the shape of the hydrophobic patch that normally binds this substrate moiety.

The orientation of **1a** in the active site anchors it tightly in position; the large bromine atom pushes against one end of the cleft and Trp21 interacts with the N3 substitution (see below) acting as a physical barrier, preventing the inhibitor from locating further up the opposite side of the cleft. There is only one hydrogen bonding interaction with the protein from N1 to the O ϵ 1 of Glu18 (2.7 Å). The bromine atom of **1a** sits in an area of the active site cleft surrounded by Gly13, Ser14, Leu17, Gly49, Val53, and Tyr110. The catalytic Cys52 is situated at this end of this region and sits 6.7 Å from the C6-bromine. In the nonliganded structure, the area in which the bromine atom binds is instead occupied by a water molecule. The large size of the subpocket around the bromine atom is consistent with analogues **16e** and **16f** that contain bicyclic aromatic substituents at C6 retaining some, albeit reduced, potency (IC₅₀ 8.0 and 8.5 μ M, respectively, Table 4).

The C4-phenyl group of **1a** protrudes into the hydrophobic region formerly occupied by Met113. The phenyl group sits at an angle of 108° to the plane of the dihydroquinazoline core. In this position, the phenyl group makes an edge–face hydrophobic interaction with Tyr110, which has rotated 62° from the nonliganded structure. Although one of the weakest hydrophobic interactions,⁴¹ it still contributes binding energy to the inhibitor complex. The residues within van der Waals interacting distances (4 Å) from this phenyl group and likely to be participating in hydrophobic interactions include Met113, Trp21, Tyr110, Leu17, Phe114, and Leu120 (Figure 4A,B). The synthetic routes to substituted dihydroquinazolines that were utilized in this study (Scheme 1) result in analogues that are racemic at C4. However, the ligand binding mode described above allows only the 4S-enantiomer to effectively occupy the induced-fit subpocket created by the movement of Met113.

The methyl acetate moiety of **1a** is directed out into the active site cleft and sits 3.1 Å from Met113S δ . It is within 3.5 Å of, and stacks against, Trp21, which has pivoted about C δ 1 to move the indole group 1.0 Å closer to the inhibitor when compared to the nonliganded structure. This helps to wedge the inhibitor in

position. The C2-methyl of **1a** also stacks with Trp21C δ 1 at a distance of 3 Å, helping to stabilize the inhibitor in this position.

The binding mode of **1a** is consistent with **1i–1l** showing weak or no inhibitory activity (IC_{50} 89 to >100 μ M) against TryR (Table 1, Figure 3). These analogues contain bulky substitutions at C2 that would prevent ligand binding due to occlusion of this position by the protein. Similarly, compounds **18** and **19** (Table 4) display reduced potency (IC_{50} 53 and 24 μ M, respectively) due to a steric clash between their C8 substituents and the surface of the active site cleft (Figure 4C).

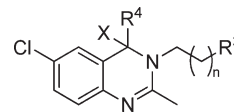
Residues Glu18, Trp21, and Met113, which form key interactions with **1a**, are not conserved in human GR (see Figure S4 of the Supporting Information), which is consistent with the fact that **1a** is not an inhibitor of the human enzyme (see above). Interestingly, the irreversible TryR inhibitor quinacrine mustard (Figure S7 of the Supporting Information) has also been shown to bind to the same hydrophobic area of the protein.²⁶ Despite binding in the same region as **1a**, the binding of quinacrine mustard does not induce a conformational change in the active site of TryR. A more detailed comparison of the TryR–dihydroquinazoline complex with the published TryR–quinacrine structures is discussed in section 3.4 of the Supporting Information.

To help rationalize the SAR derived from the dihydroquinazoline analogues, additional protein–ligand complexes were structurally characterized. To investigate the N3 substitution TryR complexes with analogues **6a**, **11e**, and **13e** were solved. Unfortunately, no complexes with analogues containing C6-aryl substitutions could be determined.

Comparison of the complexes for compounds **6a**, **11e**, and **13e** with that for **1a** show that the 3,4-dihydroquinazoline core superimposes in identical positions and that the C6-halogen substitutions overlay with one another (Figure 5). Therefore, the N3 substitution does not have any significant effect on the position of ligand binding. In analogue **6a**, the N3 acetyl ester group has been replaced with a benzyl group, resulting in a 10-fold increase in potency (**6a** IC_{50} = 0.93 μ M vs **1c** IC_{50} = 9.4 μ M). Interestingly, the benzyl group does not stack against Trp21 but is angled such that it is pointing away from the side chain of Trp21 and into the active site cleft in a similar fashion to the methyl acetate of **1a** and so does not appear to contribute to inhibitor binding. In compounds **11e** and **13e**, the ester moiety has been replaced with substituted amides, giving 11- and 22-fold improvements in potency (IC_{50} 0.86 and 0.42 μ M, respectively). In **11e** and **13e**, the N3-substituent runs along the surface of the protein, forming hydrophobic interactions with Trp21 and other residues. The displacement of water molecules from the protein surface and the resultant hydrophobic interactions are likely to be the major effect contributing to the improvement in potency observed with these analogues, as there are no other specific molecular interactions between the protein and the additional N3-amide functionality. The lack of specific molecular interactions between TryR and the N3-substituent of **11e/13e** is consistent with the relatively flat SAR observed from screening **6a–j**, **9a–f**, **11a–h**, and **13a–h** (Tables 2 and 3).

Structure-Based Inhibitor Design. Although numerous modeling studies^{15,16,21–26,42–52} have predicted binding modes for various classes of TryR inhibitors, the accuracy of these models has not been corroborated by structure-based experiments and do not consider the ability of Met113 to undergo a conformational change as observed upon binding of **1a**. Therefore, the current study represents a unique opportunity to

Table 5. C4-Substituted 3,4-Dihydroquinazoline Analogues and Their Inhibitory Activities against *T. brucei* TryR and in Cell-Based Assays



n	R ³	R ⁴	X	IC ₅₀ (μ M)		EC ₅₀ (μ M)	
				TryR	<i>T. brucei</i>	MRC5	
29a	2 NMe ₂	4-Me-Ph	H	0.23 ^a	0.73	1.9	
29b	1 N-piperidine	4 ^t Bu-Ph	H	7.9			
29c	1 N-piperidine	3-F-Ph	H	0.9	2	10	
29d	1 N-piperidine	3-OMe-Ph	H	28			
29e	1 N-piperidine	3,4-Cl ₂ -Ph	H	1.3			
29f	1 N-piperidine	cyclohexyl	H	27			
31b	1 N-piperidine	4-F-Ph	OH	8.3			
31c	1 N-piperidine	4-OMe-Ph	OH	4.9			
31d	1 N-piperidine	4-Me-Ph	OH	0.71	1.5	5.7	
32a	1 N-piperidine	4-Cl-Ph	H	0.73			
32b	1 N-piperidine	4-F-Ph	H	4.9			
32c	1 N-piperidine	4-OMe-Ph	H	1.5			
32d	1 N-piperidine	4-Me-Ph	H	0.59	1.4	5.0	
32e	1 N-piperidine	3-Cl-Ph	H	1.2			
32f	1 N-piperidine	3-Me-Ph	H	4.6			
32g	1 N-piperidine	3,4-Me ₂ -Ph	H	6.8			
34	1 N-piperidine	Bn	H	50			
35	1 N-piperidine	4-OH-Ph	H	20			
36	1 N-piperidine	4-OH-Ph	H	1.6			

^aTryR K_i = 0.19 \pm 0.01 μ M, K_i' = 1.46 \pm 0.32 μ M.

perform a validated structure-assisted inhibitor design project for TryR.

Examination of the TryR–ligand structures suggested three primary areas for further investigation: (1) the effect of altering the halogen substitution at C6, (2) challenging the hydrophobic pocket created by the movement of Met113 by altering the C4 phenyl moiety, and (3) reducing the size of the N3 substitution to improve ligand efficiency.

Comparison of the halogens and hydrogen at the C6-position (**9a**, **15b–d**) (Table 4) indicated that they were approximately equipotent. Therefore, 3,4-dihydroquinazoline-based inhibitors do not need to occupy the Ser14, Leu17, Gly49, and Val63 subpocket (Figure 4A) to effectively inhibit TryR, providing that **15b** binds in an analogous fashion to **1a**.

To investigate the effect of challenging the induced subpocket with additional steric bulk, compound **29a**, containing a *para*-toluene substituent at C4, was prepared as outlined in Scheme 4 and assayed against TryR (Table 5). The introduction of the additional methyl group resulted in a 4-fold improvement in potency (cf. **9e**, IC_{50} = 1.0 μ M, Table 2), suggesting that additional hydrophobic interactions in the subpocket are beneficial for ligand binding. Structural determination of the TryR–**29a** complex revealed that the overall effect of introducing the methyl group is to push the inhibitor further out into the active site by 0.5 Å (Figure 5). The C6-chlorine and N1 atoms act as anchor points, having moved only 0.5 Å, whereas the C4-aryl

ring has moved outward by 1.0 Å toward the mouth of the active site. To accommodate this outward movement, the phenol side chain of Tyr110 rotates through 30°. The combination of this side chain rotation and inhibitor translation brings the phenyl group of **29a** closer to Tyr110 by 0.5 Å when compared to compounds **1a**, **6a**, **11e**, and **13e** (Figure 5), allowing stronger hydrophobic stacking interactions to occur. Therefore, the 4-fold improvement in potency can be attributed to stronger hydrophobic interactions from occupying more of the subpocket and being closer to Tyr110. A more detailed kinetic analysis of **29a** revealed that its mode of inhibition is linear mixed with respect to trypanothione, compared to linear competitive for **1a**. However, comparison of the K_i and K_i' values for **29a** (Table 5) shows that **29a** has a greater affinity to the free enzyme than to the enzyme–T[S]₂ complex and so is behaving in a similar manner to **1a**.

To further explore the subpocket, a small collection of analogues containing a C4-aryl (**29b–e**, **32a–g**, **35**, and **36**), a C4-cyclohexyl (**29f**), or a C4-benzyl (**34**) substituent were prepared and tested (Table 5). All of the analogues in this collection contained an *N*-ethylpiperidine substitution at N3 in order to make them directly comparable to the majority of the other dihydroquinazolines prepared in this study. The *ortho*-substituted analogue **1d** was known to be inactive (Table 1), probably due to the additional steric bulk of the *ortho*-chlorine atom, preventing the C4 substituent from occupying the induced-fit subpocket. Therefore, all of the phenyl derivatives were substituted at the *meta* and/or *para* positions. However, none of the aryl analogues (**29b–e**, **32a–c**, **32e–g**, **35**, and **36**) showed any improvement in potency compared to the *para*-tolyl analogue **32d** (Table 5). Increasing the size of the *para*-substituent to a *tert*-butyl group (**29b**) gives an analogue which retains activity, albeit less active than the *para*-hydrogen analogue (**9a**). This suggests that either the induced-fit pocket can accommodate larger hydrophobic groups or that the ligand can bind further away from the top surface of the induced subpocket, although either hypothesis must result in suboptimal ligand binding. This is supported by the observation that the *para*-methoxy and *para*-chloro analogues (**32c** and **32a**) are equipotent to **9a**. The *meta*-methoxy analogue **29d** is 15-fold less active than **9a**, suggesting that the protein cannot readily accommodate additional steric bulk in that region of the subpocket. There is no clear relationship between the electronic character of the aryl substituent and TryR inhibitory activity, with the *meta*-fluoro (**29c**) and *para*-fluoro (**32b**) displaying a 5-fold difference in potency, which cannot be attributed to sterics. The 4-cyclohexyl analogue **29f** is 15-fold less active than the 4-Ph analogue (**9a**), consistent with the observation that a 4-aryl substituent contributes to binding affinity by forming an edge–face interaction with Tyr110. Similarly, the 4-benzyl analogue **34** is less potent than **9a**. Three of the 4-OH intermediates on the route to the 3,4-dihydroquinazolines (**31b–d**, Scheme 5) were also assayed against TryR (Table 5) and found to retain activity, albeit at a slightly reduced level compared to their reduced counterparts (**32b–d**, respectively). This is consistent with the observed binding mode of the ligands, which suggests that the additional hydroxyl group would point out into the solvent exposed active site and as a result neither enhance nor impede ligand binding.

The SAR (Figure S3 of the Supporting Information) and TryR–ligand complexes suggest that the N3-substituent makes no significant contribution to inhibitor binding. Therefore, quinazolines **6k** and **21**, which have truncated N3-substituents,

were assayed against TryR and found to be equipotent with analogues containing large R³-groups (**6a–j**, **9a–f**, Table 2). The reduction in substitution size results in compounds with improved ligand efficiencies (**6k** = 0.41 kcal mol⁻¹ per non-H atom) and reduced polar surface area.

Cell Screening. Selected dihydroquinazoline analogues were screened against both bloodstream form *T. brucei* parasites and MRC5 cells in whole cell assays (Tables 2–5). Analogues were selected such that representative examples of each array were screened. For the larger arrays, the most potent TryR inhibitors were preferentially triaged to the cell assays.

All of the dihydroquinazoline analogues that were screened demonstrated antitrypanosomal activity greater than that for the hit compound (**1a**), consistent with them all being more potent TryR inhibitors. However, there is a poor correlation between the TryR IC₅₀ and the *T. brucei* EC₅₀, with some analogues (**9a**, **15c**, **16a**) having *T. brucei* EC₅₀ values lower than their corresponding IC₅₀ values. This suggests that some analogues are not exerting all of their antitrypanosomal activity through inhibition of TryR. The selectivity within the series (as judged by MRC5 EC₅₀/*T. brucei* EC₅₀) varies from ~1 to ~20, the poor selectivity of some analogues being consistent with off-target activities. It is hoped that, as this series is further optimized against TryR there will be a concomitant reduction in the off-target effects and an increase in selectivity. Alternatively, the detailed understanding of the ligand binding mode may facilitate the identification of alternative inhibitor scaffolds with greater selectivity.

It is possible to identify some trends from analysis of the cell screening data. The nature of the N3-substituent has a large effect upon both the selectivity and *T. brucei* EC₅₀:TryR IC₅₀ ratio. Most analogues which contain a basic N3-functionality (**9c,e**, **11e,h**, and **13e,h**) have poor selectivity (0.92–2.3). In addition, the amide-containing analogues (**11e,h** and **13e,h**) display the largest (>15-fold) drop off between their enzyme and cellular inhibition values. However, **9a**, which contains an ethylpiperidine N3-substituent, does not follow this trend, instead being 11-fold selective. Analogues lacking a basic substitution at N3 (**1a**, **6a,d,g**) show reduced cell activity in both assays, suggesting that overall the amine substituent is increasing off-target activity or is important for cellular uptake. However, although the N3 moiety has an effect upon selectivity and IC₅₀:EC₅₀ ratio within the series, it does not make any significant contributions to TryR binding (Figure 5).

Compounds **9a**, **15c**, and **15d**, which vary only in their C6-halogen substituent, all display similar activities in all assays (Table 4). However, analogue **15b** (R₆ = H) is ~10-fold less potent against *T. brucei* and as a result significantly less selective. This suggests that the nonspecific antitrypanosomal activity is in part related to the hydrophobicity of the inhibitors (calculated LogD pH 7.4; **15b** = 2.1, **15d** = 3.2). Compound **16a**, which contained a C6 phenyl substituent, is 10-fold more potent against *T. brucei* cells than it is against TryR (Table 4), identifying this inhibitor as acting primarily off-target. In addition, **16a** is also one of the most potent analogues in the MRC5 assay.

Dihydroquinazoline **29a**, the most potent analogue against TryR (K_i = 0.19 μM, K_i' = 1.46 μM), is also one of the most potent against *T. brucei* (EC₅₀ = 0.73 μM), demonstrating that improved TryR potency can drive antitrypanosomal activity. All C4-substituted analogues (**29a,c**, **31d**, and **32d**) retain their antitrypanosomal activity (Table 5 cf. **9a**), in contrast with analogues containing large N3-substitutions (**11e,h** and **13e,h**, Table 3),

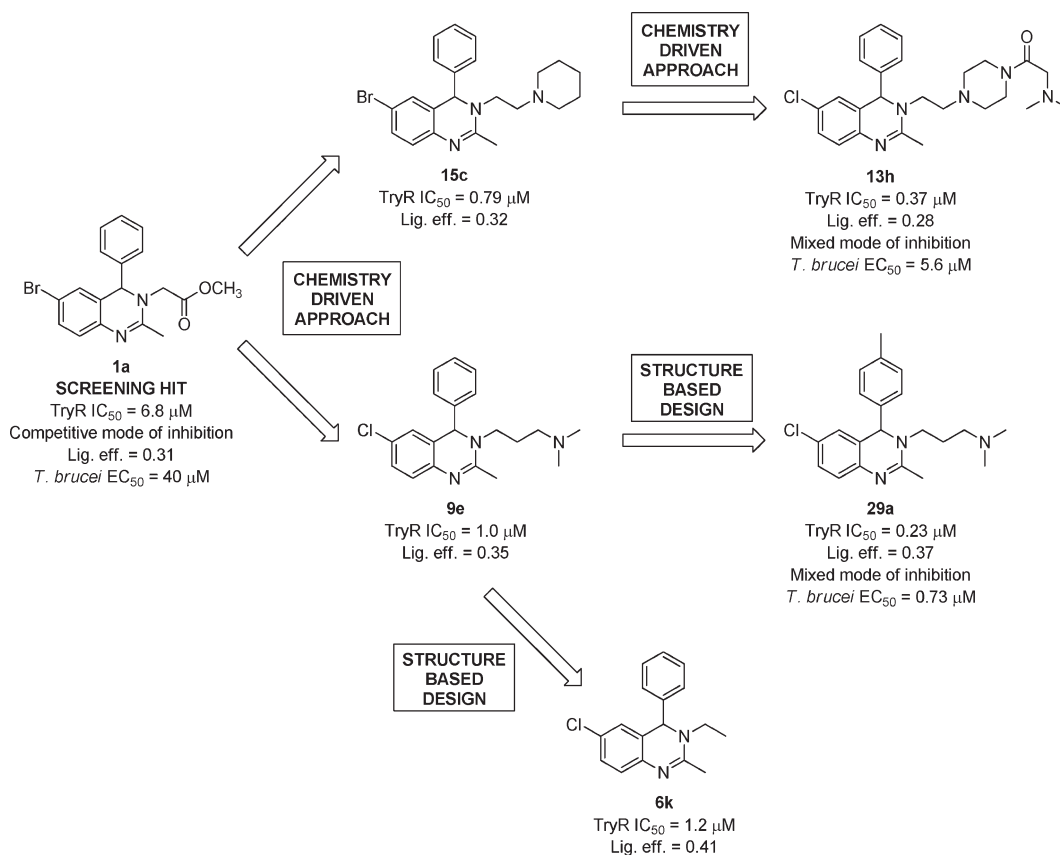


Figure 6. Summary of the development of hit compound **1a** by an initial chemistry-driven approach and subsequent structure-based inhibitor design strategy. The units for ligand efficiencies (Lig. eff.) are kcal mol^{-1} per non-hydrogen atom.

despite both sets of compounds having similar TryR inhibitory activities (Tables 3 and 5).

The current level of antitrypanosomal activity and selectivity against mammalian cells is insufficient to test these compounds in an animal model of infection. Therefore, continued development is required to identify a lead compound from this hit series.

CONCLUSIONS

Large and open active site pockets such as that found in TryR are difficult targets to effectively inhibit with small drug-like molecules. To date, no high-resolution, noncovalent enzyme–inhibitor complexes of TryR have been structurally characterized, further limiting attempts to develop potent, low molecular weight inhibitors. In this study, we have reported the crystal structures of *T. brucei* TryR in complex with a noncovalently bound inhibitor series based around a 3,4-dihydroquinazoline scaffold. In addition, the structure of *T. brucei* TryR in complex with the cofactors FAD, NADPH, and reduced trypanothione is presented. The results describe a novel and small hydrophobic pocket generated upon inhibitor binding that lies within a “privileged” region of the large active site pocket. It is anticipated that these results will facilitate the area of TryR inhibitor design and assist in the generation of further protein–inhibitor complex structures which until now have relied mainly on in silico modeling and docking studies. Given the urgent need for new HAT therapeutics, we hope that the structural information reported herein will accelerate the development of TryR inhibitors and possibly identify new drug leads.

In addition to the crystallographic studies, we have reported the identification and characterization of a novel TryR inhibitor series based upon the 3,4-dihydroquinazoline ring system. From hit compounds **1a** and **1b**, a systematic SAR study has expanded the series to include >75 analogues (Tables 1–5, Figures 3 and 6, and Figure S3 of the Supporting Information). A chemistry-driven approach was used to identify compounds which were more potent than **1a** in both the TryR biochemical and *T. brucei* cell assays (cf. **1a** and **13h**, Figure 6). However, the analogues developed by this strategy contained large N3-substitutions, resulting in high molecular weight inhibitors which were unsuitable for further optimization. The structural elucidation of ligand–TryR complexes allowed us to subsequently adopt a structure-based inhibitor design approach, which was used to develop compounds with both improved TryR and *T. brucei* inhibitory activities (cf. **1a** and **29a**, Figure 6) while maintaining ligand efficiencies $>0.3 \text{ kcal mol}^{-1}$ per non-H atom (**6k**, **29a**, Figure 6). As the dihydroquinazoline series underwent development, the mode of inhibition changed from competitive to mixed (cf. **1a** and **13h/29a**, Figure 6 and see Figure S2 of the Supporting Information). The development of a mixed inhibitor is potentially advantageous, as these are more resistant to substrate accumulation, a feature that could be important due to the high intracellular concentration of trypanothione.

To our knowledge, compound **29a** is the most potent, drug-like inhibitor of TryR reported to date. However, this series requires further optimization to improve its cellular potency and selectivity. Because of their high ligand efficiencies and low molecular weights, analogues **29a** and **6k** represent good starting

points for further structure-based drug design. The hit-to-lead development of the 3,4-dihydroquinazoline inhibitor series is summarized in Figure 6.

EXPERIMENTAL SECTION

Chemicals and solvents were purchased from the Aldrich Chemical Co., Fluka, ABCR, VWR, Acros, Fisher Chemicals, and Alfa Aesar and were used as received unless otherwise stated. Air- and moisture-sensitive reactions were carried out under an inert atmosphere of argon in oven-dried glassware. Analytical thin-layer chromatography (TLC) was performed on precoated TLC plates (layer 0.20 mm silica gel 60 with fluorescent indicator UV254, from Merck). Developed plates were air-dried and analyzed under a UV lamp (UV254/365 nm). Flash column chromatography was performed using prepacked silica gel cartridges (230–400 mesh, 40–63 μm , from SiliCycle) using a Teledyne ISCO Combiflash Companion, or Combiflash Retrieve. ^1H NMR, ^{13}C NMR, ^{19}F NMR, and 2D-NMR spectra were recorded on a Bruker Avance DPX 500 spectrometer (^1H at 500.1 MHz, ^{13}C at 125.8 MHz, ^{19}F at 470.5 MHz). Chemical shifts (δ) are expressed in ppm recorded using the residual solvent as the internal reference in all cases. Signal splitting patterns are described as singlet (s), doublet (d), triplet (t), quartet (q), multiplet (m), broad (br), or a combination thereof. Coupling constants (J) are quoted to the nearest 0.5 Hz. LC-MS analyses were performed with either an Agilent HPLC 1100 series connected to a Bruker Daltonics MicrOTOF or an Agilent Technologies 1200 series HPLC connected to an Agilent Technologies 6130 quadrupole LC/MS, where both instruments were connected to an Agilent diode array detector. LCMS chromatographic separations were conducted with a Waters Xbridge C18 column, 50 mm \times 2.1 mm, 3.5 μm particle size; mobile phase, water/acetonitrile +0.1% HCOOH, or water/acetonitrile +0.1% NH_3 ; linear gradient 80:20 to 5:95 over 3.5 min, and then held for 1.5 min; flow rate 0.5 mL min^{-1} . All assay compounds had a measured purity of $\geq 95\%$ as determined using this analytical LC-MS system (TIC and UV). High resolution electrospray measurements were performed on a Bruker Daltonics MicrOTOF mass spectrometer. Microwave-assisted chemistry was performed using a Biotage Initiator microwave synthesizer.

Method A (Compounds 3a–e). Pyridine (1.2 equiv) was added to a solution of the relevant 2-aminobenzophenone analogue, DMAP (cat.), and the relevant acid chloride in anhydrous CH_2Cl_2 and stirred at 25 $^\circ\text{C}$ for 16 h. The reaction mixture was then added to a solution of NaOH (2.0M, aq), the layers separated, and the aqueous extracted with CH_2Cl_2 . The organic layers were combined, dried over MgSO_4 , filtered, and the solvent removed under reduced pressure to give the crude amide product.

Method B (Compounds 4a–k, 7a–e). The required amine (1.2 equiv) was added to a solution of the relevant benzophenone analogue in EtOH and the reaction mixture heated at 160 $^\circ\text{C}$ for 1 h in a microwave reactor.

Method C1 (Compounds 5a–c,h,i, 8a,b). NaBH_4 (20 equiv) was added to a solution of the appropriate imine in anhydrous DMF (2 mL) and heated at 60 $^\circ\text{C}$ for 16 h. The reaction was then quenched by the addition of water (1 mL) and subsequently extracted into Et_2O (3 \times 5 mL). The workup was completed as outlined in method A. Note that the amine products were observed to slowly convert to the cyclic amidines when in solution.

Method C2 (Compounds 6d–g,j,k 9a,c–e). NaBH_4 (20 equiv) was added to a solution of the appropriate imine in EtOH and heated at 78 $^\circ\text{C}$ for 16–48 h. The reaction was then quenched by the addition of an aqueous solution of citric acid (10% w/v), the EtOH removed under reduced pressure, and the pH of the remaining aqueous adjusted to ~ 10 before being extracted with CH_2Cl_2 . The workup was completed as outlined in method A.

Method D (Compounds 6a–c,h,i, 9a,b). POCl_3 (5 equiv) was added to a solution of the relevant amine in CHCl_3 and heated at 61 $^\circ\text{C}$ for 16–24 h. The reaction mixture was added to a solution of NaOH (2.0M, aq), the layers separated, and the aqueous extracted with CH_2Cl_2 . The workup was completed as outlined in method A.

Method E (Compounds 11b–h and 13b–h). HCl (4.0 M in dioxane, 40 equiv) was added to a solution of Boc protected amine 11a or 13a in anhydrous THF and stirred at 25 $^\circ\text{C}$ for 2.5 h before removal of the solvent under reduced pressure. The crude amine was then redissolved in CH_2Cl_2 /pyridine (4:1), to which was added DMAP (cat.) and the relevant benzoyl chloride (2 equiv). The reaction was subsequently heated at 40 $^\circ\text{C}$ for 16 h, after which the reaction mixture was added to a solution of NaOH (2.0M, aq), the layers separated and the aqueous extracted with CH_2Cl_2 . The workup was completed as outlined in method A.

Method F (Compounds 18, 19a–f). $\text{Pd}(\text{PPh}_3)_4$ (0.03 equiv) was added to a degassed solution consisting of the relevant aryl bromide, the relevant boronic acid, and K_3PO_4 (2 equiv) in dioxane/water (10:1). Subsequently, the reaction was heated at 120 $^\circ\text{C}$ for 30 min in a microwave reactor, followed by evaporation of the solvents under reduced pressure.

Method G (Compounds 26b–e). *n*-BuLi (19.4 mmol, 1.6 M in hexanes, 12.1 mL) was added to a solution of the relevant aryl bromide (17.6 mmol) in anhydrous Et_2O (20 mL) at -78 $^\circ\text{C}$. Subsequently, the reaction was allowed to warm to 0 $^\circ\text{C}$ over 2 h, after which a solution of 5-chloro anthranilate (23) (4 mmol, 686 mg) in dry THF (30 mL) was added to the resultant aryl lithium and the reaction stirred for a further 2 h at 0 $^\circ\text{C}$. Work up was initiated by the addition of TMSCl (10 mL), and the reaction was allowed to warm to 25 $^\circ\text{C}$ over 15 min. Subsequently, 1N HCl (aq, 30 mL) was added and the mixture stirred at 25 $^\circ\text{C}$ for a further 15 min. The biphasic mixture was then separated and the aqueous layer neutralized and extracted into Et_2O (3 \times 50 mL). The workup was completed as outlined in method A.

Method H (Compounds 31a–g). The appropriate Grignard reagent (8 mmol) was added to a solution of quinazolinone (30) (2 mmol, 612 mg) in anhydrous THF (10 mL) at 0 $^\circ\text{C}$. The reaction was then allowed to warm to 25 $^\circ\text{C}$ over 2 h before workup was initiated by the addition of NaCl solution (satd aq 20 mL). The resultant mixture was filtered and the solids washed with EtOAc (2 \times 10 mL). Subsequently, the biphasic filtrate was separated and the pH of the aqueous layer adjusted to 10 prior to further extraction with EtOAc (3 \times 50 mL). The workup was completed as outlined in method A.

Method I (Compounds 32b–d,g). $\text{BF}_3 \cdot \text{OEt}_2$ (40 equiv) and HSiEt_3 (40 equiv) were sequentially added to a solution of the relevant alcohol in CH_2Cl_2 and the reactions stirred at 25 $^\circ\text{C}$ for 60 h. Workup was initiated by the addition of NaCl solution (satd aq), the pH of which was adjusted to 10 prior to the layers being separated and the aqueous further extracted with CH_2Cl_2 . The workup was completed as outlined in method A.

Synthesis and Analysis of Selected Compounds. *N*-(2-Benzoyl-4-chlorophenyl)acetamide (3a). Prepared according to method A from 2-amino-5-chlorobenzophenone (2a) (23.2 g, 100 mmol) and acetyl chloride (9.42 g, 120 mmol). The crude product was purified by recrystallization from EtOAc/hexane to give a white solid (21.5 g, 79%). ^1H NMR (500 MHz, CDCl_3): δ 10.63 (br s, 1H, NH), 8.61 (d, 1H, $J = 9.0$ Hz, H-6), 7.71–7.69 (m, 2H, 2 \times ArH), 7.66–7.62 (m, 1H, ArH), 7.54–7.50 (m, 4H, 4 \times ArH), 2.22 (s, 3H, CH_3). ^{13}C NMR (125 MHz, CDCl_3): δ 198.5 (C), 169.2 (C), 138.9 (C), 137.9 (C), 134.0 (CH), 133.1 (CH), 132.6 (CH), 129.9 (CH), 128.6 (CH), 127.3 (C), 124.6 (C), 123.1 (CH), 25.3 (CH_3). LRMS (ES+): m/z (%) 232 (67) [^{35}Cl M – Ac + H] $^+$, 234 (22) [^{37}Cl M – Ac + H] $^+$, 274 (100) [^{35}Cl M + H] $^+$, 276 (42) [^{37}Cl M + H] $^+$.

N-(2-((Benzylimino)(phenyl)methyl)-4-chlorophenyl)acetamide (4a). Prepared according to method B from benzylamine (129 mg,

1.2 mmol) and *N*-(2-benzoyl-4-chlorophenyl)acetamide (**3a**) (274 mg, 1 mmol) in EtOH (3 mL). Upon cooling, the product crystallized from the crude reaction mixture and was subsequently recovered by filtration and washed with cold EtOH (2 × 5 mL) to give a white crystalline solid (89 mg, 25%). ¹H NMR (500 MHz, CDCl₃): δ 13.32 (br s, 1H, NH), 8.70 (d, 1H, *J* = 9.0 Hz, ArH), 7.59–7.54 (m, 3H, 3 × ArH), 7.38–7.35 (m, 2H, 2 × ArH), 7.33–7.28 (m, 4H, 4 × ArH), 7.23–7.21 (m, 2H, 2 × ArH), 6.91 (d, 1H, *J* = 2.5 Hz, H-3), 4.51 (s, 2H, CH₂), 1.82 (s, 3H, CH₃). ¹³C NMR (125 MHz, CDCl₃): δ 171.5 (C), 169.6 (C), 139.5 (C), 139.1 (C), 135.3 (C), 132.3 (CH), 131.0 (CH), 129.3 (CH), 129.1 (CH), 128.7 (CH), 128.1 (CH), 127.4 (CH), 126.7 (C), 124.4 (C), 121.8 (CH), 57.9 (CH₂), 25.0 (CH₃). LRMS (ES⁺): *m/z* (%) 363 (100) [³⁵Cl M + H]⁺, 365 (41) [³⁷Cl M + H]⁺.

(*R/S*)-*N*-(2-((Benzylamino)(phenyl)methyl)-4-chlorophenyl)acetamide (**5a**). Prepared according to method C1 from *N*-(2-((benzylimino)(phenyl)methyl)-4-chlorophenyl)acetamide (**4a**) (109 mg, 0.3 mmol). The crude product was purified by flash column chromatography (EtOAc/hexane 0:100 → 50:50) to give a cream solid (48 mg, 44%). ¹H NMR (500 MHz, CDCl₃): δ 11.0 (br s, 1H, NH), 8.22 (d, 1H, *J* = 8.5 Hz, ArH), 7.32–7.15 (m, 10H, 10 × ArH), 7.04–7.02 (m, 1H, ArH), 6.96 (d, 1H, ArH), 4.90 (s, 1H, CH), 3.71 (s, 2H, CH₂), 1.98 (s, 3H, CH₃). LRMS (ES⁺): *m/z* (%) 365 (100) [³⁵Cl M + H]⁺, 367 (33) [³⁷Cl M + H]⁺.

(*R/S*)-3-Benzyl-6-chloro-2-methyl-4-phenyl-3,4-dihydroquinazoline (**6a**). Prepared according to method D from *N*-(2-((benzylamino)(phenyl)methyl)-4-chlorophenyl)acetamide (**5a**) (48 mg, 0.13 mmol). The crude product was purified by triturating from Et₂O (40 mg, 87%). ¹H NMR (500 MHz, CDCl₃): δ 7.69 (d, 1H, *J* = 8.5 Hz, ArH), 7.48–7.42 (m, 6H, 6 × ArH), 7.27–7.23 (m, 3H, 3 × ArH), 7.19–7.17 (m, 1H, ArH), 6.77 (d, 1H, *J* = 2.0 Hz, H-5), 5.53 (s, 1H, H-4), 4.89 (d, 1H, *J* = 16.0 Hz, CHH), 4.29 (d, 1H, *J* = 16.0 Hz, CHH), 2.81 (s, 3H, CH₃). ¹³C NMR (125 MHz, CDCl₃): δ 158.4 (C), 139.2 (C), 133.1 (C), 131.4 (C), 130.2 (CH), 130.1 (CH), 129.91 (CH), 129.88 (CH), 129.5 (CH), 128.2 (C), 127.3 (CH), 126.9 (CH), 126.8 (CH), 122.2 (C), 120.5 (CH), 62.3 (CH), 52.2 (CH₂), 18.5 (CH₃). LRMS (ES⁺): *m/z* (%) 347 (100) [³⁵Cl M + H]⁺, 349 (34) [³⁷Cl M + H]⁺. HRMS (ES⁺): calcd for C₂₂H₂₀ClN₂ [M + H]⁺ 347.1310, found 347.1299 (3.06 ppm).

N-(4-Chloro-2-(phenyl(2-(piperidin-1-yl)ethylimino)methyl)phenyl)acetamide (**7a**). Prepared according to method B from 1-(2-aminoethyl)piperidine (154 mg, 1.2 mmol) and *N*-(2-benzoyl-4-chlorophenyl)acetamide (**3a**) (274 mg, 1 mmol). The reaction solvent was removed under reduced pressure and purified by column chromatography (MeOH/CH₂Cl₂ 0:100 → 10:90) to give a white solid (210 mg, 54%). ¹H NMR (500 MHz, CDCl₃): δ 13.56 (br s, 1H, NH), 8.72 (d, 1H, *J* = 9.0 Hz, H-6), 7.51–7.45 (m, 3H, 3 × ArH), 7.29 (dd, 1H, *J* = 9.0, 3.0 Hz, H-5), 7.12–7.10 (m, 2H, 2 × ArH), 6.83 (d, 1H, *J* = 3.0 Hz, H-3), 3.43 (t, 2H, *J* = 7.0, CH₂), 2.66 (t, 2H, *J* = 7.0, CH₂), 2.37–2.28 (m, 4H, 2 × CH₂), 2.24 (s, 3H, CH₃), 1.55–1.51 (m, 4H, 2 × CH₂), 1.43–1.38 (m, 2H, CH₂). ¹³C NMR (125 MHz, CDCl₃): δ 171.8 (C), 169.6 (C), 139.2 (C), 135.5 (C), 132.1 (CH), 130.8 (CH), 129.1 (CH), 129.0 (CH), 127.1 (CH), 126.6 (C), 124.3 (C), 121.6 (CH), 60.2 (CH₂), 54.8 (CH₂), 51.1 (CH₂), 25.9 (CH₂), 25.5 (CH₃), 24.3 (CH₂). LRMS (ES⁺): *m/z* (%) 192.5 (24) [³⁵Cl M + 2H]²⁺, 384 (100) [³⁵Cl M + H]⁺, 386 (31) [³⁷Cl M + H]⁺.

(*R/S*)-6-Chloro-2-methyl-4-phenyl-3-(2-(piperidin-1-yl)ethyl)-3,4-dihydroquinazoline (**9a**). Prepared according to method C2 or method D. Method C2 from *N*-(4-chloro-2-(phenyl(2-(piperidin-1-yl)ethylimino)methyl)phenyl)acetamide (**7a**) (360 mg, 0.94 mmol) in EtOH (5 mL): The crude product was purified by flash column chromatography (0.5 M NH₃ in MeOH/CH₂Cl₂ 1:100 → 4:96) to give a cream solid (211 mg, 61%). Method D from *N*-(4-chloro-2-(phenyl(2-(piperidin-1-yl)ethylamino)methyl)phenyl)acetamide (**8a**) (16 mg, 0.04 mmol): Work up gave a colorless semisolid (11 mg, 71%) that required

no further purification. ¹H NMR (500 MHz, CDCl₃): δ 7.32–7.24 (m, 5H, 5 × ArH), 7.05 (dd, 1H, *J* = 8.5, 2.5 Hz, H-7), 6.99 (d, 1H, *J* = 8.5 Hz, H-8), 6.74 (d, 1H, *J* = 2.5 Hz, H-5), 5.53 (s, 1H, H-4), 3.43 (ddd, 1H, *J* = 14.5, 8.5, 6.0 Hz, CHH), 3.16 (ddd, 1H, *J* = 14.5, 8.5, 6.0 Hz, CHH), 2.50 (ddd, 1H, *J* = 12.5, 8.5, 6.0 Hz, CHH), 2.38–2.28 (m, 5H, CHH eand 2 × CH₂), 2.26 (s, 3H, CH₃), 1.55–1.51 (m, 4H, 2 × CH₂), 1.43–1.37 (m, 2H, CH₂). ¹³C NMR (125 MHz, CDCl₃): δ 156.4 (C), 143.7 (C), 139.6 (C), 129.1 (CH), 128.7 (C), 128.4 (CH), 128.3 (CH), 126.7 (CH), 126.3 (C), 126.0 (CH), 125.0 (CH), 63.2 (CH), 57.4 (CH₂), 55.1 (CH₂), 46.9 (CH₂), 26.0 (CH₂), 24.2 (CH₂), 22.4 (CH₃). LRMS (ES⁺): *m/z* (%) 184.5 (88) [³⁵Cl M + 2H]²⁺, 185.5 (35) [³⁷Cl M + 2H]²⁺, 368 (100) [³⁵Cl M + H]⁺, 370 (35) [³⁷Cl M + H]⁺. HRMS (ES⁺): calcd for C₂₂H₂₇ClN₃ [M + H]⁺ 368.1888, found 368.1888 (−0.01 ppm).

(*R/S*)-*tert*-Butyl 2-(6-Chloro-2-methyl-4-phenylquinazolin-3(4H)-yl)ethylcarbamate (**11a**). Two identical reactions containing *N*-(2-benzoyl-4-chlorophenyl)acetamide (**3a**) (1.37 g, 5.0 mmol) and *N*-Boc-(2-aminoethyl)amine (1.19 mL, 7.5 mmol) in EtOH (20 mL) were reacted according to method B. The two reactions were then combined and diluted with EtOH (60 mL) and reacted directly according to method C2. The product was purified by column chromatography (MeOH/CH₂Cl₂ 2:98 → 10:90) to give a white solid (1.19 g, 30%). ¹H NMR (500 MHz, CDCl₃): δ 7.33–7.26 (m, 5H, 5 × ArH), 7.08 (dd, 1H, *J* = 8.5, 2.0 Hz, H-7), 7.05 (d, 1H, *J* = 8.5 Hz, H-8), 6.76 (d, 1H, *J* = 2.0 Hz, H-5), 5.44 (s, 1H, H-4), 3.57–3.52 (m, 1H, CHH), 3.25–3.14 (m, 3H, CHH and CH₂), 2.25 (s, 3H, CH₃), 1.40 (s, 9H, 3 × CH₃). ¹³C NMR (125 MHz, DMSO-*d*₆): δ 156.6 (C), 155.9 (C), 143.3 (C), 129.3 (CH), 129.1 (C), 128.6 (CH), 128.5 (CH), 126.6 (CH), 126.1 (CH), 126.0 (C), 125.0 (CH), 79.9 (C), 62.5 (CH), 48.4 (CH₂), 38.2 (CH₂), 28.3 (CH₃), 22.3 (CH₃). LRMS (ES⁺): *m/z* (%) 400 (100) [³⁵Cl M + H]⁺, 402 (41) [³⁷Cl M + H]⁺. HRMS (ES⁺): calcd for C₂₂H₂₇N₃O₂ [M + H]⁺ 400.1786, found 400.1796 (−2.33 ppm).

(*R/S*)-*N*-(2-(6-Chloro-2-methyl-4-phenylquinazolin-3(4H)-yl)ethyl)benzamide (**11d**). Prepared according to method E from *tert*-butyl 2-(6-chloro-2-methyl-4-phenylquinazolin-3(4H)-yl)ethylcarbamate (**11a**) (120 mg, 0.3 mmol) and benzoyl chloride (84 mg, 0.6 mmol). The product was purified by flash column chromatography (0.5 M NH₃ MeOH/CH₂Cl₂ 0:100 → 10:90) to give a clear glass (53 mg, 44%). ¹H NMR (500 MHz, CDCl₃): δ 7.68–7.66 (m, 2H, 2 × ArH), 7.53–7.50 (m, 1H, ArH), 7.44–7.41 (m, 2H, 2 × ArH), 7.36–7.30 (m, 5H, 5 × ArH), 7.11 (dd, 1H, *J* = 8.5, 2.5 Hz, H-7), 7.06 (d, 1H, *J* = 8.5 Hz, H-8), 6.78 (d, 1H, *J* = 2.5 Hz, H-5), 6.27 (br s, 1H, NH), 5.47 (s, 1H, H-4), 3.68–3.43 (m, 4H, 2 × CH₂), 2.29 (s, 3H, CH₃). ¹³C NMR (125 MHz, DMSO-*d*₆): δ 168.0 (C), 156.5 (C), 143.6 (C), 139.4 (C), 133.7 (C), 132.0 (CH), 129.3 (CH), 129.2 (C), 128.8 (CH), 128.63 (CH), 128.55 (CH), 126.8 (CH), 126.5 (CH), 126.1 (C), 126.0 (CH), 125.3 (CH), 63.0 (CH), 48.5 (CH₂), 38.3 (CH₂), 22.6 (CH₃). LRMS (ES⁺): *m/z* (%) 404 (100) [³⁵Cl M + H]⁺, 406 (35) [³⁷Cl M + H]⁺. HRMS (ES⁺): calcd for C₂₄H₂₃N₃O₁ [M + H]⁺ 404.1524, found 404.1520 (1.01 ppm).

Synthesis of (2-Amino-5-bromophenyl)(phenyl)methanone (2c). NBS (1.87 g, 10.5 mmol) was added to a suspension of 2-aminobenzophenone (1.97 g, 10 mmol) and toxic acid-derivatized silica gel (0.68 mmol/g, 150 mg) in MeCN/Et₂O (1:3, 50 mL). The reaction mixture was stirred for 30 min, filtered, the silica washed with CH₂Cl₂ (10 mL), and the combined filtrate removed under reduced pressure. The crude aryl bromide was purified by flash column chromatography (CH₂Cl₂) to give a yellow solid (2.25 g, 82%). ¹H NMR (500 MHz, CDCl₃): δ 7.66–7.64 (m, 2H, 2 × ArH), 7.60–7.57 (m, 2H, 2 × ArH), 7.52–7.49 (m, 2H, 2 × ArH), 7.38 (dd, 1H, *J* = 8.5, 2.0 Hz, H-4), 6.67 (d, 1H, *J* = 8.5 Hz, H-3), 6.11 (br s, 2H, NH₂). ¹³C NMR (125 MHz, CDCl₃): δ 198.0 (C), 149.7 (C), 139.3 (C), 136.9 (CH), 136.2 (CH), 131.6 (CH), 129.1 (CH), 128.4 (CH), 119.4 (C), 118.8 (CH), 106.6 (C). LRMS (ES⁺): *m/z* (%) 276 (100) [⁷⁹Br M + H]⁺, 278 (100) [⁸¹Br M + H]⁺.

Synthesis of (*R/S*)-2-Methyl-4,6-diphenyl-3-(2-(piperidin-1-yl)ethyl)-3,4-dihydroquinazoline (**16a**). Prepared according to method F from 6-bromo-2-methyl-4-phenyl-3-(2-(piperidin-1-yl)ethyl)-3,4-dihydroquinazoline (**15c**) (41 mg, 0.1 mmol) and phenylboronic acid (18 mg, 0.15 mmol). The crude product was purified by flash column chromatography (0.5 M NH₃ (MeOH)/CH₂Cl₂ 0:100 → 10:90) to give a brown solid (26 mg, 63%). ¹H NMR (500 MHz, CDCl₃): δ 7.48–4.46 (m, 2H, 2 × ArH), 7.40–7.30 (m, 7H, 7 × ArH), 7.28–7.24 (m, 2H, 2 × ArH), 7.18 (d, 1H, J = 8.0 Hz, ArH), 7.03 (d, 1H, J = 2.5 Hz, ArH), 5.65 (s, 1H, H-4), 3.51 (ddd, 1H, J = 15.0, 9.0, 6.0 Hz, CHH), 3.23 (ddd, 1H, J = 15.0, 9.0, 6.0 Hz, CHH), 2.57 (ddd, 1H, J = 12.5, 9.0, 5.5 Hz, CHH), 2.44–2.31 (m, 8H, CHH, 2 × CH₂, CH₃), 1.59–1.54 (m, 4H, 2 × CH₂), 1.46–1.41 (m, 2H, CH₂). LRMS (ES+): *m/z* (%) 410 (100) [M + H]⁺. HRMS (ES+): calcd for C₂₈H₃₂N₃ [M + H]⁺ 410.2591, found 410.2599 (–2.08 ppm).

(*R/S*)-3-(6-Chloro-2-methyl-4,8-diphenylquinazolin-3(4H)-yl)-*N,N*-dimethylpropan-1-amine (**19**). Prepared according to general method E from 3-(6-bromo-8-chloro-2-methyl-4-phenylquinazolin-3(4H)-yl)-*N,N*-dimethylpropan-1-amine (**18**) (42 mg, 0.1 mmol) and phenylboronic acid (12 mg, 0.1 mmol). The crude product was purified by preparative HPLC to give a white solid (17 mg, 41%). ¹H NMR (500 MHz, CDCl₃): δ 7.64–7.62 (m, 2H, 2 × ArH), 7.41–7.37 (m, 2H, 2 × ArH), 7.32–7.25 (m, 6H, 6 × ArH), 7.16 (d, 1H, J = 2.5 Hz, ArH), 6.79 (dd, 1H, J = 2.5, 0.5 Hz, ArH), 5.48 (s, 1H, CH), 3.46 (ddd, 1H, J = 14.5, 8.5, 6.0 Hz, CHH), 3.11 (ddd, 1H, J = 14.5, 8.5, 6.0 Hz, CHH), 2.33–2.22 (m, 5H, CH₂ and CH₃), 2.20 (s, 6H, 2 × NCH₃), 1.82–1.65 (m, 2H, CH₂). ¹³C NMR (125 MHz, CDCl₃): δ 156.0 (C), 143.9 (C), 138.7 (C), 137.4 (C), 136.9 (C), 130.5 (CH), 129.5 (CH), 129.1 (CH), 128.3 (CH), 127.7 (CH), 127.4 (C), 127.0 (CH), 126.6 (CH), 125.1 (CH), 62.6 (CH), 56.3 (CH₂), 46.8 (CH₂), 45.4 (CH₃), 26.3 (CH₂), 22.9 (CH₃). [Note: one quaternary carbon resonance is absent, possibly due to it having an identical chemical shift to another quaternary carbon resonance]. LRMS (ES+): *m/z* (%) 209.5 (42) [³⁵Cl M + 2H]²⁺, 210.5 (13) [³⁷Cl M + 2H]²⁺, 418 (100) [³⁵Cl M + H]⁺, 420 (38) [³⁷Cl M + H]⁺. HRMS (ES+): calcd for C₂₆H₂₉Cl₁N₃ [M + H]⁺ 418.2045, found 418.2034 (2.54 ppm).

N-(4-Chloro-2-(4-methylbenzoyl)phenyl)acetamide (**27a**). *p*-Tolylmagnesium bromide (1.0 M in THF, 10 mL, 10 mmol) was slowly added to a solution of benzoxazinone (**24**) (1.96 g, 10 mmol) in anhydrous THF (40 mL) at 0 °C. The reaction mixture was allowed to warm to 25 °C over 30 min and stirred for an additional 1.5 h before the reaction was quenched by the addition of NaCl solution (satd aq 50 mL). The resultant biphasic mixture was separated and the aqueous layer extracted with EtOAc (3 × 50 mL). Subsequently, the combined organic layers were dried over MgSO₄, filtered, and the solvent removed under reduced pressure. The crude product was purified by flash column chromatography over silica (Et₂O/hexanes 0:100 → 50:50) to give a white solid (511 mg, 18%). ¹H NMR (500 MHz, CDCl₃): δ 10.54 (br s, 1H, NH), 8.57 (d, 1H, J = 9.5 Hz, ArH), 7.63–7.61 (m, 2H, AA'BB', 2 × ArH), 7.51–7.49 (m, 2H, 2 × ArH), 7.32–7.30 (m, 2H, AA'BB', 2 × ArH), 2.46 (s, 3H, CH₃), 2.21 (s, 3H, CH₃). ¹³C NMR (125 MHz, CDCl₃): δ 198.0 (CO), 169.1 (C), 144.1 (C), 138.7 (C), 135.1 (C), 133.6 (CH), 132.4 (CH), 130.2 (CH), 129.3 (CH), 127.2 (C), 125.0 (C), 123.1 (CH), 25.2 (CH₃), 21.7 (CH₃). LRMS (ES+): *m/z* (%) 288 (100) [³⁵Cl M + H]⁺, 290 (31) [³⁷Cl M + H]⁺.

N-(4-Chloro-2-((3-(dimethylamino)propylimino)(*p*-tolyl)methyl)phenyl)acetamide (**28a**). Prepared according to general method B from *N*-(4-chloro-2-(4-methylbenzoyl)phenyl)acetamide (**27a**) and 3-(dimethylamino)-1-propylamine. The crude product was purified by flash column chromatography over silica (0.5 M NH₃ in MeOH/CHCl₃ 1:99 → 4:96) to give a white solid (485 mg, 65%). ¹H NMR (500 MHz, CDCl₃): δ 13.66 (s, 1H, NH), 8.71 (d, 1H, J = 9.0 Hz, H-6), 7.29–7.25 (m, 3H, AA'BB' and H-5), 6.99–6.97 (m, 2H, AA'BB'), 6.86 (d, 1H, J = 2.5 Hz, H-3), 3.33 (t, 2H, J = 7.0 Hz, CH₂), 2.42 (s, 3H, CH₃), 2.30 (t, 2H, J = 7.5 Hz, CH₂), 2.21 (s, 3H, CH₃), 2.19 (s, 6H, 2 × CH₃),

1.89–1.84 (m, 2H, CH₂). ¹³C NMR (125 MHz, CDCl₃): δ 171.7 (C), 169.3 (C), 139.1 (C), 138.9 (C), 132.4 (C), 132.2 (CH), 130.6 (CH), 129.6 (CH), 127.1 (CH), 126.6 (C), 124.4 (C), 121.5 (CH), 57.7 (CH₂), 51.8 (CH₂), 45.6 (CH₃), 29.7 (CH₂), 25.4 (CH₃), 21.4 (CH₃). LRMS (ES+): *m/z* (%) 186.5 (100) [³⁵Cl M + 2H]²⁺, 187.5 (32) [³⁷Cl M + 2H]²⁺, 372 (61) [³⁵Cl M + H]⁺, 374 (18) [³⁷Cl M + H]⁺.

3-(6-Chloro-2-methyl-4-*p*-tolylquinazolin-3(4H)-yl)-*N,N*-dimethylpropan-1-amine (**29a**). Prepared according to general method C2 from *N*-(4-chloro-2-((3-(dimethylamino)propylimino)(*p*-tolyl)methyl)phenyl)acetamide (**28a**). The crude product was purified by flash column chromatography over silica (MeOH/CH₂Cl₂ 0:100 → 10:90) to give a clear gum (99 mg, 28%). ¹H NMR (500 MHz, CDCl₃): δ 7.20–7.17 (m, 2H, AA'BB', 2 × ArH), 7.15–7.13 (m, 2H, AA'BB', 2 × ArH), 7.09 (dd, 1H, J = 8.5, 2.5 Hz, H-7), 7.05 (d, 1H, J = 8.5 Hz, H-8), 6.77 (d, 1H, J = 2.5 Hz, H-5), 5.46 (s, 1H, H-4), 3.46 (ddd, 1H, J = 14.5, 8.0, 6.5 Hz, CHH), 3.11 (ddd, 1H, J = 14.5, 8.5, 6.0 Hz, CHH), 2.33 (s, 3H, CH₃), 2.30 (s, 3H, CH₃), 2.29–2.21 (m, 2H, CH₂), 2.20 (s, 6H, 2 × NCH₃), 1.81–1.64 (m, 2H, CH₂). ¹³C NMR (125 MHz, CDCl₃): δ 156.5 (C), 140.9 (C), 139.8 (C), 138.1 (C), 129.7 (CH), 128.7 (C), 128.2 (CH), 126.6 (CH), 126.5 (C), 126.0 (CH), 125.1 (CH), 62.1 (CH), 56.2 (CH₂), 46.8 (CH₂), 45.4 (CH₃), 26.2 (CH₂), 22.4 (CH₃), 21.1 (CH₃). LRMS (ES+): *m/z* (%) 178.5 (27) [³⁵Cl M + 2H]²⁺, 356 (100) [³⁵Cl M + H]⁺, 358 (31) [³⁷Cl M + H]⁺. HRMS (ES+): calcd for C₂₁H₂₇³⁵Cl₁N₃ [M + H]⁺ 356.1888, found 356.1881 (1.84 ppm).

2-(Amino-5-chlorophenyl)(4-*tert*-butylphenyl)methanone (**26b**). Prepared according to general method G from 1-bromo-4-(*tert*-butyl)benzene (3.75 g, 17.6 mmol). The final product was purified by flash column chromatography over silica (EtOAc/hexanes 0:100 → 50:50) to give a yellow solid (679 mg, 59%). ¹H NMR (500 MHz, CDCl₃): δ 7.61–7.58 (m, 2H, AA'BB', 2 × ArH), 7.50–7.48 (m, 2H, AA'BB', 2 × ArH), 7.47 (d, 1H, J = 2.5 Hz, H-6), 7.24 (dd, 1H, J = 9.0, 2.5 Hz, H-4), 6.69 (d, 1H, J = 9.0 Hz, H-3), 1.37 (s, 9H, 3 × CH₃). ¹³C NMR (125 MHz, CDCl₃): δ 197.8 (CO), 155.3 (C), 149.2 (C), 136.4 (C), 133.9 (CH), 133.2 (CH), 129.3 (CH), 125.3 (CH), 120.0 (C), 119.2 (C), 118.4 (CH), 35.1 (C), 31.2 (CH₃). LRMS (ES+): *m/z* (%) 288 (100) [³⁵Cl M + H]⁺, 290 (33) [³⁷Cl M + H]⁺.

4-(4-*tert*-Butylphenyl)-6-chloro-2-methyl-3-(2-(piperidin-1-yl)ethyl)-3,4-dihydroquinazoline (**29b**). Prepared in three steps from **26b**, acetyl chloride, and 1-(2-aminoethyl)piperidine following general methods A, B, and C2. The final product was purified by reverse phase preparative HPLC to give a white solid (40 mg, 6% over 3 steps). ¹H NMR (500 MHz, CDCl₃): δ 7.33–7.31 (m, 2H, AA'BB'), 7.21–7.19 (m, 2H, AA'BB'), 7.07 (dd, 1H, J = 8.5, 2.0 Hz, H-7), 7.01 (d, 1H, J = 8.5 Hz, H-8), 6.77 (d, 1H, J = 2.0 Hz, H-5), 5.51 (s, 1H, H-4), 3.45 (ddd, 1H, J = 14.5, 8.5, 6.0 Hz, CHH), 3.20 (ddd, 1H, J = 14.5, 8.5, 6.0 Hz, CHH), 2.52 (ddd, 1H, J = 13.0, 8.5, 6.0 Hz, CHH), 2.40–2.31 (m, 5H, CHH and 2 × CH₂), 2.28 (s, 3H, CH₃), 1.58–1.53 (m, 4H, 2 × CH₂), 1.45–1.40 (m, 2H, CH₂), 1.29 (s, 9H, 3 × CH₃). ¹³C NMR (125 MHz, CDCl₃): δ 156.4 (C), 151.2 (C), 140.9 (C), 139.9 (C), 128.6 (C), 128.2 (CH), 126.5 (C), 126.3 (CH), 126.0 (CH), 125.95 (CH), 125.0 (CH), 62.8 (CH), 57.4 (CH₂), 55.1 (CH₂), 46.9 (CH₂), 34.6 (C), 31.3 (CH₃), 26.0 (CH₂), 24.2 (CH₂), 22.5 (CH₃). LRMS (ES+): *m/z* (%) 424 (100) [³⁵Cl M + H]⁺, 426 (34) [³⁷Cl M + H]⁺. HRMS (ES+): calcd for C₂₆H₃₅³⁵Cl₁N₃ [M + H]⁺ 424.2514, found 424.2520 (–1.52 ppm).

6-Chloro-4-(4-chlorophenyl)-2-methyl-3-(2-(piperidin-1-yl)ethyl)-3,4-dihydroquinazolin-4-ol (**31a**). Prepared according to general method H using 4-chlorophenylmagnesium bromide (1.0 M solution in Et₂O, 8 mL, 8 mmol). The final product was purified by recrystallization from MeCN to give a white solid (339 mg, 41%). ¹H NMR (500 MHz, CDCl₃): δ 9.48 (br s, 1H, OH), 7.49–7.46 (m, 2H, AA'BB', 2 × ArH), 7.35–7.32 (m, 2H, AA'BB', 2 × ArH), 7.14 (dd, 1H, J = 8.5, 2.5 Hz, H-7), 7.11 (d, 1H, J = 8.5 Hz, H-8), 6.79 (d, 1H, J = 2.5 Hz, H-5), 3.51–3.47 (m, 1H, CHH), 3.10–3.05 (m, 1H, CHH), 2.60–2.55 (m, 1H, CHH), 2.50–2.45 (m, 2H, 2 × CHH), 2.35–2.31 (m, 3 × CHH

and CH₃), 1.72–1.68 (m, 4H, 2 × CH₂), 1.54–1.48 (m, 2H, CH₂). ¹³C NMR (125 MHz, CDCl₃): δ 153.5 (C), 145.4 (C), 138.2 (C), 133.9 (C), 129.10 (C), 129.08 (C), 128.7 (CH), 128.5 (CH), 128.1 (CH), 127.4 (CH), 125.4 (CH), 85.2 (C), 58.9 (CH₂), 54.6 (CH₂), 43.9 (CH₂), 25.2 (CH₂), 23.6 (CH₂), 23.2 (CH₃). LRMS (ES+): *m/z* (%) 418 (100) [³⁵Cl₂ M + H]⁺, 420 (64) [³⁵Cl ³⁷Cl M + H]⁺.

6-Chloro-4-(4-chlorophenyl)-2-methyl-3-(2-(piperidin-1-yl)ethyl)-3,4-dihydroquinazoline (32a). Prepared according to general method I from dihydroquinazolinol (31a) (42 mg, 0.1 mmol). The final product was purified from the crude reaction mixture by flash column chromatography over silica (MeOH/CH₂Cl₂ 0:100 → 10:90) to give a clear glass (31 mg, 77%). ¹H NMR (500 MHz, CDCl₃): δ 7.35–7.33 (m, 2H, AA'BB', 2 × ArH), 7.25–7.22 (m, 2H, AA'BB', 2 × ArH), 7.15–7.11 (m, 2H, H-7 and H-8), 6.78 (d, 1H, *J* = 1.5 Hz, H-5), 5.76 (s, 1H, H-4), 3.52 (ddd, 1H, *J* = 15.0, 6.5, 6.5 Hz, CHH), 3.29–3.24 (m, 1H, CHH), 2.59–2.53 (m, 1H, CHH), 2.48–2.26 (m, 8H, CHH, CH₃ and 2 × CH₂), 1.57–1.53 (m, 4H, 2 × CH₂), 1.44–1.39 (m, 2H, CH₂). ¹³C NMR (125 MHz, CDCl₃): δ 157.5 (C), 140.7 (C), 135.0 (C), 130.6 (C), 129.70 (CH), 129.2 (CH), 128.2 (CH), 126.2 (CH), 124.4 (C), 122.9 (CH), 62.9 (CH), 57.2 (CH₂), 55.1 (CH₂), 47.3 (CH₂), 26.0 (CH₂), 24.0 (CH₂), 21.0 (CH₃). Note: HMBC analysis suggests that the quaternary carbon peak at 135.0 results from two quaternary carbon atoms. LRMS (ES+): *m/z* (%) 402 (100) [³⁵Cl₂ M + H]⁺, 404 (71) [³⁵Cl ³⁷Cl M + H]⁺. HRMS (ES+): calcd for C₂₂H₂₆³⁵Cl₂N₃ [M + H]⁺ 402.1498, found 402.1501 (−0.62 ppm).

Biology. *TryR Enzyme Assay.* Compounds were assayed against recombinant TryR from *T. brucei brucei* strain S427, which was expressed and purified as previously described.³⁵ Potency was determined as independent duplicates for all compounds tested as previously.^{9,12} A serial titration of clomipramine was used as a positive control in each assay plate: BTCP was used as an additional control in some screening plates. ActivityBase from IDBS was used for all data processing and analysis. Some inhibitors were screened in a 96-well format essentially as above. The assay was assessed for robustness, yielding the following typical performance statistics: *Z'* = 0.84 ± 0.001; %CV (plate) = 3.65 ± 0.4; S:B = 10 ± 0.25; IC₅₀ (clomipramine) = 12.4 ± 0.14 μm. All reported IC₅₀ values are the mean of at least two replicates, with the standard deviations typically being less than 20% of the mean.

Cell Assays. Compounds were assayed against bloodstream form *T. brucei brucei* and MRC5 cells using resazurin fluorescence-based viability assays as previously described. All reported EC₅₀ values are the mean of at least two replicates, with the standard deviations typically being less than 50% of the mean. The HAT drug pentamidine was present in all *T. brucei* plates as a positive control. Pentamidine has an EC₅₀ of 5 nM (*n* > 1000) in this assay, which is in close agreement with published EC₅₀ values.³⁷

Mode of Inhibition Studies. These were determined as previously described using a DTNB-coupled assay.¹² Briefly, the assay mixture contained 150 μM NADPH, 50 μM DTNB, and 20 mU mL^{−1} TryR and was initiated by the addition of T[S]₂ ranging from 0.58 to 50 μM. The linear rate of increase in absorbance at 412 nm was determined using a Molecular Devices Thermomax plate reader. Each data set was fitted by nonlinear regression to the Michaelis–Menten equation using GraFit 5.0 (Erithacus software). The resulting individual fits were examined as Lineweaver–Burke transformations and the graphs inspected for diagnostic inhibition patterns. The entire data set was then globally fitted to the appropriate equation (competitive, mixed, or uncompetitive inhibition) and goodness-of-fit between models compared using the F-test (see Figure S2 of the Supporting Information for an example).

Cloning, Expression, and Purification of His-Tagged TryR. The gene corresponding to *T. brucei* trypanothione reductase was cloned into a pET15b vector (Novagen) for overexpression with a 6-histidine tag. The plasmid was transformed into *Escherichia coli* strain BL21 (DE3) codon plus RIL. Cells were cultured in autoinduction media for 3 days and

harvested by centrifugation. The cell pellet was resuspended in 25 mM Tris-HCl, pH 8.0, 500 mM NaBr, and 5 mM imidazole and lysed using a French Press at 16000 psi. Insoluble debris was removed by centrifugation at 40000g for 20 min and the soluble lysate clarified by filtration through a 0.2 μm syringe filter. Ni²⁺ affinity chromatography, thrombin removal of the 6-histidine tag, and Q Sepharose anion exchange chromatography on an Akta purifier (GE Healthcare) yielded 80 mg L^{−1} of purified protein as assessed by SDS-PAGE. The protein was dialyzed into 50 mM HEPES, pH 7.5, 50 mM NaBr, and concentrated to 15 mg mL^{−1} to be used for crystallography.

Crystallization. Sparse matrix screens (Jena Biosciences) were used to identify initial crystallization conditions, which were optimized and refined using the hanging drop vapor diffusion method to 26% MPD, 10% polyethylene glycol 3350, and 40 mM imidazole, pH 8.0. Thin, plate-type crystals grew in 3 days with dimensions 0.3 × 0.2 × 0.05 mm³. The crystallization mother liquor acted as a suitable cryoprotectant during data collection in which the crystals were cooled to 100 K in a stream of nitrogen gas. For the inhibitor complex structures, crystals were soaked for between 2 and 24 h with solid inhibitor compound introduced into the hanging crystallization drops. Data were collected both in-house on a Rigaku 007 MicroMax rotating anode X-ray generator coupled to an R-Axis IV++ image plate detector and at the European Synchrotron Radiation Facility on beamlines ID14–2 and ID14–4. The crystals were space group *P*₂₁ with cell dimensions of *a* = 101.8, *b* = 63.6, *c* = 169.8 Å, β = 97.9°. Data were processed and scaled using the XDS package,^{53,54} and statistics are shown in Table S1 of the Supporting Information.

Structure Solution, Model Building, And Refinement. The structure of nonliganded *T. brucei* TryR was solved by molecular replacement using MOLREP (CCP4) and the *T. cruzi* TryR model 1aog²⁰ [82% sequence identity]. Matthews coefficient calculations implied that there were two dimers in the asymmetric unit with a solvent content of 51%, which were found by MOLREP. COOT⁵⁵ was used to correct the nonidentical residues in the TryR model chain A, which was then superposed on chain B, C, and D to generate the two dimers in the asymmetric unit. Further model building and water placement with COOT was interspersed with refinement with REFMAC5. The nonliganded protein was used as a template to solve the complex structures of the inhibitor series and other ligands in the study. Coordinates and libraries for the different inhibitors were generated with PRODRG.^{56,57} Statistics for each of the complex structures are shown in Table S1 of the Supporting Information.

■ ASSOCIATED CONTENT

S Supporting Information. Additional synthetic procedures and analytical information for screening compounds and selected intermediates. Further discussion of the protein X-ray crystal structures. All scheme, figure, table and section numbers prefixed with an 'S' are present in the Supporting Information. This material is available free of charge via the Internet at <http://pubs.acs.org>.

Accession Codes

Coordinates of *T. brucei* TryR and TryR-ligand complexes have been deposited at the RSCB Protein Data Bank, (PDB ID codes 2woi, 2wov, 2wow, 2wp5, 2wp6, 2wpc, 2wpe, 2wvf).

■ AUTHOR INFORMATION

Corresponding Author

*Phone: (44)1382-385155. Fax: (44)1382-385542. E-mail: a.h.fairlamb@dundee.ac.uk.

Author Contributions

⁵These authors contributed equally to the work.

ACKNOWLEDGMENT

We thank Gina McKay for performing high resolution mass spectrometry analyses and for assistance with performing other NMR and MS analyses, Daniel James, for data management, Dr. Sandra Oza for cloning the His-tagged *T. brucei* TryR, Irene Hallyburton and Bhavya Rao for enzyme and cell screening assays, Daniel Spinks and Dr. Laura Cleghorn for synthetic investigations and compound selection during the early stages of this research programme, and staff at the European Synchrotron Radiation Facility for support with synchrotron data collection. A.H.F. is a Wellcome Principle Research Fellow, funded by grants from the Wellcome Trust (WT 07938, WT 077705 and WT 083481). Additional funding was provided by the Scottish Funding Council.

ABBREVIATIONS USED

BTCP, 1-(1-(benzo[*b*]thiophen-2-yl)cyclohexyl)piperidine; DMAP, 4-(dimethylamino)pyridine; DMF, *N,N*-dimethylformamide; DTNB, 5,5'-dithiobis(2-nitrobenzoic acid); ES+, electrospray positive ionization; GR, glutathione reductase; HAT, human African trypanosomiasis; HRMS, high-resolution mass spectrum; LRMS, low-resolution mass spectrum; MPD, (\pm)-2-methyl-2,4-pentanediol; NBS, *N*-bromosuccinimide; SAR, structure-activity relationship; THF, tetrahydrofuran; TMSCl, chlorotri-methylsilane; TryR, trypanothione reductase

REFERENCES

- (1) Stuart, K. D.; Brun, R.; Croft, S. L.; Fairlamb, A. H.; Gurtler, R. E.; McKerrow, J. H.; Reed, S.; Tarleton, R. L. Kinetoplastids: related protozoan pathogens, different diseases. *J. Clin. Invest.* **2008**, *118*, 1301–1310.
- (2) Nwaka, S.; Hudson, A. Innovative lead discovery strategies for tropical diseases. *Nature Rev. Drug Discovery* **2006**, *5*, 941–955.
- (3) Fairlamb, A. H.; Cerami, A. Metabolism and functions of trypanothione in the Kinetoplastida. *Annu. Rev. Microbiol.* **1992**, *46*, 695–729.
- (4) Augustyns, K.; Amssoms, K.; Yamani, A.; Rajan, P. K.; Haemers, A. Trypanothione as a target in the design of antitrypanosomal and antileishmanial agents. *Curr. Pharm. Des.* **2001**, *7*, 1117–1141.
- (5) Krauth-Siegel, R. L.; Bauer, H.; Schirmer, H. Dithiol proteins as guardians of the intracellular redox milieu in parasites: old and new drug targets in trypanosomes and malaria-causing plasmodia. *Angew. Chem., Int. Ed. Engl.* **2005**, *44*, 690–715.
- (6) Faerman, C. H.; Savvides, S. N.; Strickland, C.; Breidenbach, M. A.; Ponasik, J. A.; Ganem, B.; Ripoll, D.; Krauth-Siegel, R. L.; Karplus, P. A. Charge is the major discriminating factor for glutathione reductase versus trypanothione reductase inhibitors. *Bioorg. Med. Chem.* **1996**, *4*, 1247–1253.
- (7) Krauth-Siegel, R. L.; Comini, M. A. Redox control in trypanosomatids, parasitic protozoa with trypanothione-based thiol metabolism. *Biochim. Biophys. Acta* **2008**, *1780*, 1236–1248.
- (8) Krieger, S.; Schwarz, W.; Ariyanayagam, M. R.; Fairlamb, A. H.; Krauth-Siegel, R. L.; Clayton, C. Trypanosomes lacking trypanothione reductase are avirulent and show increased sensitivity to oxidative stress. *Mol. Microbiol.* **2000**, *35*, 542–552.
- (9) Spinks, D.; Shanks, E. J.; Cleghorn, L. A.; McElroy, S.; Jones, D.; James, D.; Fairlamb, A. H.; Frearson, J. A.; Wyatt, P. G.; Gilbert, I. H. Investigation of trypanothione reductase as a drug target in *Trypanosoma brucei*. *ChemMedChem* **2009**, *4*, 2060–2069.
- (10) Frearson, J. A.; Wyatt, P. A.; Gilbert, I. H.; Fairlamb, A. H. Target assessment for antiparasitic drug discovery. *Trends Parasitol.* **2007**, *23*, 589–595.
- (11) Eberle, C.; Burkhard, J. A.; Stump, B.; Kaiser, M.; Brun, R.; Krauth-Siegel, R. L.; Diederich, F. Synthesis, inhibition potency, binding mode, and antiprotozoal activities of fluorescent inhibitors of trypanothione reductase based on mepacrine-conjugated diaryl sulfide scaffolds. *ChemMedChem* **2009**, *4*, 2034–2044.
- (12) Patterson, S.; Jones, D. C.; Shanks, E. J.; Frearson, J. A.; Gilbert, I. H.; Wyatt, P. G.; Fairlamb, A. H. Synthesis and evaluation of 1-(1-(benzo[*b*]thiophen-2-yl)cyclohexyl)piperidine (BTCP) analogues as inhibitors of trypanothione reductase. *ChemMedChem* **2009**, *4*, 1341–1353.
- (13) Holloway, G. A.; Charman, W. N.; Fairlamb, A. H.; Brun, R.; Kaiser, M.; Kostewicz, E.; Novello, P. M.; Parisot, J. P.; Richardson, J.; Street, I. P.; Watson, K. G.; Baell, J. B. Trypanothione reductase high-throughput screening campaign identifies novel classes of inhibitors with anti-parasitic activity. *Antimicrob. Agents Chemother.* **2009**, *53*, 2824–2833.
- (14) Holloway, G. A.; Baell, J. B.; Fairlamb, A. H.; Novello, P. M.; Parisot, J. P.; Richardson, J.; Watson, K. G.; Street, I. P. Discovery of 2-iminobenzimidazoles as a new class of trypanothione reductase inhibitor by high-throughput screening. *Bioorg. Med. Chem. Lett.* **2007**, *17*, 1422–1427.
- (15) Stump, B.; Eberle, C.; Kaiser, M.; Brun, R.; Krauth-Siegel, R. L.; Diederich, F. Diaryl sulfide-based inhibitors of trypanothione reductase: inhibition potency, revised binding mode and antiprotozoal activities. *Org. Biomol. Chem.* **2008**, *6*, 3935–3947.
- (16) Parveen, S.; Khan, M. O. F.; Austin, S. E.; Croft, S. L.; Yardley, V.; Rock, P.; Douglas, K. T. Antitrypanosomal, antileishmanial, and antimalarial activities of quaternary arylalkylammonium 2-amino-4-chlorophenyl phenyl sulfides, a new class of trypanothione reductase inhibitor, and of *N*-acyl derivatives of 2-amino-4-chlorophenyl phenyl sulfide. *J. Med. Chem.* **2005**, *48*, 8087–8097.
- (17) Dixon, M. J.; Maurer, R. I.; Biggi, C.; Oyarzabal, J.; Essex, J. W.; Bradley, M. Mechanism and structure-activity relationships of norspermidine-based peptidic inhibitors of trypanothione reductase. *Bioorg. Med. Chem.* **2005**, *13*, 4513–4526.
- (18) Lee, B.; Bauer, H.; Melchers, J.; Ruppert, T.; Rattray, L.; Yardley, V.; Davioud-Charvet, E.; Krauth-Siegel, R. L. Irreversible inactivation of trypanothione reductase by unsaturated mannich bases: a divinyl ketone as key intermediate. *J. Med. Chem.* **2005**, *48*, 7400–7410.
- (19) Girault, S.; Davioud-Charvet, E.; Maes, L.; Dubremetz, J. F.; Debreu, M. A.; Landry, V.; Sergheraert, C. Potent and specific inhibitors of trypanothione reductase from *Trypanosoma cruzi*: bis(2-aminodiphenylsulfides) for fluorescent labeling studies. *Bioorg. Med. Chem.* **2001**, *9*, 837–846.
- (20) Zhang, Y.; Bond, C. S.; Bailey, S.; Cunningham, M. L.; Fairlamb, A. H.; Hunter, W. N. The crystal structure of trypanothione reductase from the human pathogen *Trypanosoma cruzi* at 2.3 Å resolution. *Protein Sci.* **1996**, *5*, 52–61.
- (21) Benson, T. J.; McKie, J. H.; Garforth, J.; Borges, A.; Fairlamb, A. H.; Douglas, K. T. Rationally designed selective inhibitors of trypanothione reductase: phenothiazines and related tricyclics as lead structures. *Biochem. J.* **1992**, *286*, 9–11.
- (22) Perez-Pineiro, R.; Burgos, A.; Jones, D. C.; Andrew, L. C.; Rodriguez, H.; Suarez, M.; Fairlamb, A. H.; Wishart, D. S. Development of a novel virtual screening cascade protocol to identify potential trypanothione reductase inhibitors. *J. Med. Chem.* **2009**, *52*, 1670–1680.
- (23) Khan, M. O. F.; Austin, S. E.; Chan, C.; Yin, H.; Marks, D.; Vaghjani, S. N.; Kendrick, H.; Yardley, V.; Croft, S. L.; Douglas, K. T. Use of an additional hydrophobic binding site, the Z site, in the rational drug design of a new class of stronger trypanothione reductase inhibitor, quaternary alkylammonium phenothiazines. *J. Med. Chem.* **2000**, *43*, 3148–3156.
- (24) Venkatesan, S. K.; Shukla, A. K.; Dubey, V. K. Molecular docking studies of selected tricyclic and quinone derivatives on trypanothione reductase of *Leishmania infantum*. *J. Comput. Chem.* **2010**, *31*, 2463–2475.

- (25) Cavalli, A.; Lizzi, F.; Bongarzone, S.; Brun, R.; Krauth-Siegel, R. L.; Bolognesi, M. L. Privileged structure-guided synthesis of quinazolinone derivatives as inhibitors of trypanothione reductase. *Bioorg. Med. Chem. Lett.* **2009**, *19*, 3031–3035.
- (26) Saravanamuthu, A.; Vickers, T. J.; Bond, C. S.; Peterson, M. R.; Hunter, W. N.; Fairlamb, A. H. Two interacting binding sites for quinacrine derivatives in the active site of trypanothione reductase—a template for drug design. *J. Biol. Chem.* **2004**, *279*, 29493–29500.
- (27) Yamamoto, M.; Yamamoto, H. Synthetic studies on quinazolinone derivatives. 2. The reactions of 2-trichloroacetamidobenzophenones and 2-trifluoroacetamidobenzophenones with primary amines. *Chem. Pharm. Bull. (Tokyo)* **1981**, *29*, 2135–2156.
- (28) Das, B.; Venkateswarlu, K.; Krishnaiah, M.; Holla, H. An efficient, rapid and regioselective nuclear bromination of aromatics and heteroaromatics with NBS using sulfonic-acid-functionalized silica as a heterogeneous recyclable catalyst. *Tetrahedron Lett.* **2006**, *47*, 8693–8697.
- (29) Miyaura, N.; Suzuki, A. Palladium-catalyzed cross-coupling reactions of organoboron compounds. *Chem. Rev.* **1995**, *95*, 2457–2483.
- (30) Jiang, J. B.; Hesson, D. P.; Dusak, B. A.; Dexter, D. L.; Kang, G. J.; Hamel, E. Synthesis and biological evaluation of 2-styrylquinazolin-4(3H)-ones, A new class of antimetabolic anticancer agents which inhibit tubulin polymerization. *J. Med. Chem.* **1990**, *33*, 1721–1728.
- (31) Okabe, M.; Sun, R. C. Improved synthesis of 2-amino-5-chlorophenyl-2'-pyrrolketone, a key intermediate in the synthesis of HIV Tat-antagonists. *Tetrahedron* **1995**, *51*, 1861–1866.
- (32) Fryer, R. I.; Zhang, P. W.; Rios, R. The synthesis of substituted 2-aminophenyl heterocyclic ketones. *Synth. Commun.* **1993**, *23*, 985–992.
- (33) Kostakis, I. K.; Elomri, A.; Seguin, E.; Iannelli, M.; Besson, T. Rapid synthesis of 2,3-disubstituted-quinazolin-4-ones enhanced by microwave-assisted decomposition of formamide. *Tetrahedron Lett.* **2007**, *48*, 6609–6613.
- (34) Zimaity, T.; Anwar, M.; Abdelhay, F. I.; Abdelmegeed, M. F. Study of reaction of Grignard reagents with 4-(3H)-quinazolinones and 4H-3,1-benzoxazin-4-ones. *Acta Chim. Acad. Sci. Hung.* **1975**, *87*, 251–255.
- (35) Jones, D. C.; Ariza, A.; Chow, W. H.; Oza, S. L.; Fairlamb, A. H. Comparative structural, kinetic and inhibitor studies of *Trypanosoma brucei* trypanothione reductase with *T. cruzi*. *Mol. Biochem. Parasitol.* **2010**, *169*, 12–19.
- (36) Hamilton, C. J.; Saravanamuthu, A.; Eggleston, I. M.; Fairlamb, A. H. Ellman's-reagent-mediated regeneration of trypanothione in situ: substrate-economical microplate and time-dependent inhibition assays for trypanothione reductase. *Biochem. J.* **2003**, *369*, 529–537.
- (37) Jones, D. C.; Hallyburton, I.; Stojanovski, L.; Read, K. D.; Frearson, J. A.; Fairlamb, A. H. Identification of a kappa-opioid agonist as a potent and selective lead for drug development against human African trypanosomiasis. *Biochem. Pharmacol.* **2010**, *80*, 1478–1486.
- (38) Raz, B.; Iten, M.; Grether-Buhler, Y.; Kaminsky, R.; Brun, R. The Alamar Blue assay to determine drug sensitivity of African trypanosomes (*Tb. rhodesiense* and *Tb. gambiense*) in vitro. *Acta Trop.* **1997**, *68*, 139–147.
- (39) Hopkins, A. L.; Groom, C. R.; Alex, A. Ligand efficiency: a useful metric for lead selection. *Drug Discovery Today* **2004**, *9*, 430–431.
- (40) Bailey, S.; Fairlamb, A. H.; Hunter, W. N. Structure of trypanothione reductase from *Crithidia fasciculata* at 2.6 Å resolution—enzyme–NADP interactions at 2.8 Å resolution. *Acta Crystallogr., Sect. D: Biol. Crystallogr.* **1994**, *50*, 139–154.
- (41) Waters, M. L. Aromatic interactions in model systems. *Curr. Opin. Chem. Biol.* **2002**, *6*, 736–741.
- (42) Chan, C.; Yin, H.; Garforth, J.; McKie, J. H.; Jaouhari, R.; Speers, P.; Douglas, K. T.; Rock, P. J.; Yardley, V.; Croft, S. L.; Fairlamb, A. H. Phenothiazine inhibitors of trypanothione reductase as potential antitrypanosomal and antileishmanial drugs. *J. Med. Chem.* **1998**, *41*, 148–156.
- (43) Garforth, J.; Yin, H.; McKie, J. H.; Douglas, K. T.; Fairlamb, A. H. Rational design of selective ligands for trypanothione reductase from *Trypanosoma cruzi*. Structural effects on the inhibition by dibenzazepines based on imipramine. *J. Enzyme Inhib.* **1997**, *12*, 161–173.
- (44) Horvath, D. A virtual screening approach applied to the search for trypanothione reductase inhibitors. *J. Med. Chem.* **1997**, *40*, 2412–2423.
- (45) Iribarne, F.; Paulino, M.; Aguilera, S.; Murphy, M.; Tapia, O. Docking and molecular dynamics studies at trypanothione reductase and glutathione reductase active sites. *J. Mol. Model.* **2002**, *8*, 173–183.
- (46) Lee, M. G. S.; E, Y.; Axelrod, N. Construction of trypanosome artificial mini-chromosomes. *Nucleic Acids Res.* **1995**, *23*, 4893–4899.
- (47) Martinez-Merino, V.; Cerecetto, H. CoMFA-SIMCA model for antichagasic nitrofurazone derivatives. *Bioorg. Med. Chem.* **2001**, *9*, 1025–1030.
- (48) Jacoby, E. M.; Schlichting, I.; Lantwin, C. B.; Kabsch, W.; Krauth-Siegel, R. L. Crystal structure of the *Trypanosoma cruzi* trypanothione reductase–mepacrine complex. *Proteins* **1996**, *24*, 73–80.
- (49) Meiering, S.; Inhoff, O.; Mies, J.; Vincek, A.; Garcia, G.; Kramer, B.; Dormeyer, M.; Krauth-Siegel, R. L. Inhibitors of *Trypanosoma cruzi* trypanothione reductase revealed by virtual screening and parallel synthesis. *J. Med. Chem.* **2005**, *48*, 4793–4802.
- (50) Paulino, M.; Iribarne, F.; Hansz, M.; Vega, M.; Seoane, G.; Cerecetto, H.; Di Maio, R.; Caracelli, I.; Zukerman-Schpector, J.; Olea, C.; Stoppani, A. O. M.; Berriman, M.; Fairlamb, A. H.; Tapia, O. Computer assisted design of potentially active anti-trypanosomal compounds. *J. Mol. Struct. (THEOCHEM)* **2002**, *584*, 95–105.
- (51) Prieto, J. J.; Talevi, A.; Bruno-Blanch, L. E. Application of linear discriminant analysis in the virtual screening of antichagasic drugs through trypanothione reductase inhibition. *Mol. Diversity* **2006**, *10*, 361–375.
- (52) Salmon-Chemin, L.; Buisine, E.; Yardley, V.; Kohler, S.; Debreu, M. A.; Landry, V.; Sergheraert, C.; Croft, S. L.; Krauth-Siegel, R. L.; Davioud-Charvet, E. 2- and 3-Substituted 1,4-naphthoquinone derivatives as subversive substrates of trypanothione reductase and lipamide dehydrogenase from *Trypanosoma cruzi*: synthesis and correlation between redox cycling activities and in vitro cytotoxicity. *J. Med. Chem.* **2001**, *44*, 548–565.
- (53) Kabsch, W. Evaluation of single-crystal X-ray-diffraction data from a position-sensitive detector. *J. Appl. Crystallogr.* **1988**, *21*, 916–924.
- (54) Kabsch, W. XDS. *Acta Crystallogr., Sect. D: Biol. Crystallogr.* **2010**, *66*, 125–132.
- (55) Emsley, P.; Cowtan, K. Coot: model-building tools for molecular graphics. *Acta Crystallogr., Sect. D: Biol. Crystallogr.* **2004**, *60*, 2126–2132.
- (56) Schuttelkopf, A. W.; van Aalten, D. M. PRODRG: a tool for high-throughput crystallography of protein–ligand complexes. *Acta Crystallogr., Sect. D: Biol. Crystallogr.* **2004**, *60*, 1355–1363.
- (57) van Aalten, D. M.; Bywater, R.; Findlay, J. B.; Hendlich, M.; Hoof, R. W.; Vriend, G. PRODRG, a program for generating molecular topologies and unique molecular descriptors from coordinates of small molecules. *J. Comput.-Aided. Mol. Des.* **1996**, *10*, 255–262.